Available online at www.sciencedirect.com
SCIENCE DIRECT®
Journal of Computational Physics 214 (2006) 698–724
JOURNAL OF COMPUTATIONAL PHYSICS
www.elsevier.com/locate/jcp

High order residual distribution conservative finite difference WENO schemes for steady state problems on non-smooth meshes

Ching-Shan Chou, Chi-Wang Shu *

Division of Applied Mathematics, Brown University, Box F, Providence, RI 02912, USA

Received 24 July 2005; received in revised form 8 October 2005; accepted 13 October 2005
Available online 28 November 2005

Abstract

In this paper, we propose a high order residual distribution conservative finite difference scheme for solving steady state hyperbolic conservation laws on non-smooth Cartesian or other structured curvilinear meshes. WENO (weighted essentially non-oscillatory) integration is used to compute the numerical fluxes based on the point values of the solution, and the principles of residual distribution schemes are adapted to obtain steady state solutions. In two space dimension, the computational cost of our scheme is comparable to that of a high order WENO finite difference scheme and is therefore much lower than that of a high order WENO finite volume scheme, yet the new scheme does not have the restriction on mesh smoothness of the traditional high order conservative finite difference schemes. A Lax–Wendroff type theorem is proved for convergence towards weak solutions in one and two dimensions, and extensive numerical experiments are performed for one- and two-dimensional scalar problems and systems to demonstrate the quality of the new scheme, including high order accuracy on non-smooth meshes, conservation, and non-oscillatory properties for solutions with shocks and other discontinuities.

Keywords: Residual distribution; Fluctuation splitting; WENO integration; High order accuracy; Conservation laws

1. Introduction

High order conservative schemes, such as finite volume and finite difference methods, are widely used in solving hyperbolic conservation laws

$$u_t + \nabla \cdot F(u) = 0, \tag{1.1}$$

where hyperbolicity means that $\frac{\partial F(u)}{\partial u} \cdot \xi$ is diagonalizable with real eigenvalues for any real vector ξ. In finite volume schemes, the conservative unknowns are the cell averages, which are updated by evaluating the fluxes

* Corresponding author. Tel.: +1 401 863 2549; fax: +1 401 863 1355.
E-mail addresses: cschou@dam.brown.edu (C.-S. Chou), shu@dam.brown.edu (C.-W. Shu).

0021-9991/$ - see front matter
doi:10.1016/j.jcp.2005.10.007

through reconstructions. In finite difference schemes, we update the point values, and reconstructions are also needed when evaluating the fluxes. In both types of schemes, high order accurate essentially non-oscillatory (ENO) and weighted essentially non-oscillatory (WENO) reconstructions [17,28,29,20,18,26] are very successful in capturing shocks in a sharp, non-oscillatory fashion while maintaining high order accuracy in smooth regions.

For one-dimensional problems, high order conservative finite volume and finite difference schemes have comparable computational cost. However, for two- or three-dimensional problems on Cartesian or general curvilinear meshes, multi-dimensional reconstructions are needed to approximate the integrals for the numerical fluxes for finite volume schemes, while in finite difference schemes, the reconstructions can be performed dimension-by-dimension. Therefore, finite difference schemes are much less expensive in computational costs than finite volume schemes of the same order of accuracy. For a detailed comparison of these two types of schemes, we refer to [10,27]. On the other hand, there are some drawbacks in using high order finite difference schemes, and the most significant one is the restriction on the smoothness of the meshes. To obtain a high order conservative finite difference scheme, the mesh size is required to be uniform or at least smoothly varying [21]. In this respect, finite volume schemes are much more flexible. To partially overcome this restriction, a multi-domain finite difference WENO scheme is proposed in [25]. Even though this multi-domain approach is performing well in many complicated applications [25,19], it does have the drawback that it is no longer strictly conservative.

In this paper, we are interested in developing high order conservative schemes which are of the finite difference type (the numerical approximations are the point values of the solution) and have a comparable computational cost as regular finite difference schemes, yet the meshes are allowed to be arbitrary Cartesian or curvilinear without any smoothness assumption. Our effort is restricted to steady state problems in this paper. Time dependent problems are significantly more difficult and will be left for future work. In order to obtain conservative high order finite difference schemes on such more general meshes, we need to start from a different point of view other than directly approximating the derivatives by a conservative flux difference (as it is shown in [21] that such conservative flux difference approximation can be at most second order accurate on general non-smooth meshes). The idea of "residual distribution" comes into play here naturally. A brief overview of a residual distribution scheme for a two-dimensional conservation law (1.1) is given as follows. We are given a general triangular or quadrilateral mesh, with n_t elements $\{T_j\}_{j=1,\ldots,n_t}$ and n_s nodes $\{M_i\}_{i=1,\ldots,n_s}$ which are the vertices of these elements. The residual Φ^T over the element T is defined and decomposed as

$$\Phi^T = \int_T \mathrm{div} F^h(u_h)\,\mathrm{d}x, \qquad \sum_{i,M_i\in T} \Phi_i^T = \Phi^T, \tag{1.2}$$

where F^h is an approximation of the flux function F in (1.1), and the total residual Φ^T over the element T is decomposed to a sum of residuals Φ_i^T to be distributed to each node M_i of T. The design principles for the distribution of the residual are described in [1]. The dual cells, C_i, $i = 1,\ldots,n_s$ are obtained by joining the centroids of the elements T_j having M_i as one of the nodes, to the mid-points of the edges of T_j. If we denote the collection of elements T_j having M_i as one of the nodes as S_i, then the residual distribution scheme is given as

$$u_i^{n+1} = u_i^n - \frac{\Delta t_n}{|C_i|} \sum_{T\in S_i} \Phi_i^T. \tag{1.3}$$

The class of residual distribution (RD) schemes, or fluctuation splitting schemes for solving steady state problems (solutions to (1.1) which are time independent), has received considerable attention. Such schemes were pioneered by Deconinck et al. [12], Roe and Sidilkover [23], Struijs et al. [30] and followed by later works in, e.g. [1,3,32,7]. The RD schemes use a pointwise representation of the solution, same as in finite difference schemes, and it allows conservative approximations with high order accuracy on very general meshes. The RD schemes are demonstrated to be robust in many numerical tests. A Lax–Wendroff type theorem has been provided to ensure convergence to weak solutions [5], and stability is established following maximum principles, see, e.g. [1,7]. The accuracy at steady state is ensured if the scheme satisfies the residual property, which is related to the accuracy approximating the residuals, see [1]. Most of the works mentioned above are for

schemes of at most second order accuracy. Following the systematic construction from a first order monotone and upwind RD scheme to a second order one, Abgrall and Roe [8] proposed a natural generalization to obtain a high order RD scheme on general triangular meshes. For a hybrid of different meshes, quadrilateral meshes have also been considered [31], and a recent work by Abgrall and Marpeau [4] gives a formal construction of second order schemes on quadrilateral meshes. Besides steady state problems, attention has also been paid recently to design RD schemes for unsteady problems [11,6].

Most of the previous works emphasize the construction of second order accurate RD schemes on general triangular or quadrilateral meshes, although an enhancement to higher order accuracy is possible. In our work, we are interested in designing high order finite difference schemes on structured curvilinear meshes which are not necessarily smooth. In fact, we only consider in this paper rectangular meshes or a special class of quadrilateral meshes formed by parallelograms. The main purpose of this restriction on the meshes is the observation that the evaluation of the residuals in Eq. (1.2) in 2D, which are in general two-dimensional integrals, can be decomposed to a dimension-by-dimension one-dimensional computation. We would like to remark that our construction and distribution of the residual are somewhat different from the usual residual distribution schemes by starting from a stable monotone first order scheme and then upgrading the accuracy, rather we compute directly a high order accurate residual by a WENO integration procedure and rely on the residual distribution stage to obey the upwinding property for numerical stability. As for the residual distribution, we follow the RD schemes with a modification. A Lax–Wendroff type theorem for convergence towards weak solutions is proved, similar to that in [4], but with a wider stencil. It should be emphasized that our purpose is to save computational cost in the evaluation of the residual via a dimension-by-dimension approach on structured curvilinear meshes, instead of improving the distribution mechanism.

This paper is organized as follows. In Section 2, we present the fourth order central WENO integration on one-dimensional non-smooth meshes as an example of high order WENO integration. In Sections 3 and 4, we describe the residual evaluation procedure through a WENO integration and the residual distribution procedure for one and two-dimensional problems, respectively. Section 5 contains extensive numerical simulation results for one and two-dimensional scalar and system steady state problems to demonstrate the good behavior of our scheme. Concluding remarks are given in Section 6. The Lax–Wendroff type theorem for convergence towards weak solutions is proven for the one-dimensional case in Section 3 and for the two-dimensional case in Appendix A.

2. Introduction of the WENO integration

In this section, we first introduce one-dimensional WENO integration which is an important component of the residual evaluation in (1.2) for our special meshes. Given a grid $\{x_j\}_{j=0,\ldots,N} \subset [a,b]$, which is not assumed to be uniform or smooth, we define cells and cell sizes by $I_{j+\frac{1}{2}} = [x_j, x_{j+1}]$, $\Delta x_{j+\frac{1}{2}} = x_{j+1} - x_j$, $j = 0,\ldots,N-1$. Consider a real-valued function $u(x)$ defined on $[a,b]$ and denote $u_j = u(x_j)$, $j = 0,\ldots,N$, we would like to approximate the integral of $u(x)$ on $I_{i+\frac{1}{2}}$ to $(2k-1)$th order accuracy.

In each stencil $S_r(i) = \{x_{i-r},\ldots,x_{i-r+k-1}\}$ which contains $I_{i+\frac{1}{2}}$, there is a unique polynomial $p_r(x)$ of degree at most $k-1$ which interpolates $u(x)$ at the nodes in $S_r(i)$. We denote the integral of $p_r(x)$ on $I_{i+\frac{1}{2}}$ by $v^{(r)}$, hence

$$v^{(r)} = \sum_{j=0}^{k-1} c_{i-r+j} u_{i-r+j}, \quad r = 0,\ldots,k-2, \tag{2.1}$$

where the coefficients c_{i-r+j} depend on the cell sizes in $S_r(i)$ but not on u.

The WENO integration would take a convex combination of all the $v^{(r)}$ defined in Eq. (2.1) as a new approximation to the integral $\int_{I_{i+\frac{1}{2}}} u(x)\,dx$

$$v = \sum_{r=0}^{k-2} \omega_r v^{(r)}.$$

We require $\omega_r \geqslant 0$ and $\sum_{r=0}^{k-2} \omega_r = 1$ for stability and consistency.

To determine ω_r, recall that if $u(x)$ is smooth in all candidate stencils, there are constants d_r such that

$$v = \sum_{r=0}^{k-2} d_r v^{(r)} = \int_{I_{i+\frac{1}{2}}} u(x)\,\mathrm{d}x + \mathrm{O}(\Delta x^{2k-1}),$$

where $\sum_{r=0}^{k-2} d_r = 1$. In this smooth case, we would hope to have $\omega_r = d_r + \mathrm{O}(\Delta x^{k-1}),\ r = 0,\ldots,k-2$ so that $(2k-1)$th order accuracy can be achieved for the integral. When the function $u(x)$ has a discontinuity in one or more of the stencils, we would hope the corresponding weights ω_r to be essentially 0 to avoid spurious oscillations. A way to produce ω_r, same as in the original WENO reconstructions [18,26], is the following:

$$\omega_r = \frac{\alpha_r}{\sum_{s=0}^{k-2}\alpha_s}, \quad r = 0,\ldots,k-2$$

with

$$\alpha_r = \frac{d_r}{(\epsilon+\beta_r)^2}.$$

Here, $\epsilon > 0$ is introduced to avoid the denominator to become 0, and we take $\epsilon = 10^{-6}$ in our numerical test. β_r is the so-called "smoothness indicator" of the stencil $S_r(i)$ which measures the smoothness of the function $u(x)$ in the stencil and is defined by

$$\beta_r = \sum_{l=1}^{k-1} \int_{x_i}^{x_{i+1}} \left(\Delta x_{i+\frac{1}{2}}\right)^{2l-1} \left(\frac{\partial^l p_r(x)}{\partial^l x}\right)^2 \mathrm{d}x.$$

Near boundary, one-side biased rather than central stencils could be used in the WENO procedure. More details about the WENO procedure can be found in [18].

3. High order RD finite difference WENO schemes in one dimension

In this section, we design a residual distribution high order WENO finite difference scheme for one-dimensional steady state problems on non-smooth meshes. In the first subsection, we define the residuals from the integral form, as in Eq. (1.2), and then describe the distribution of the residuals, complying with the principles of upwinding and the residual property. We also state and prove a Lax–Wendroff type theorem for convergence towards weak solutions. In the second subsection, we extend the scheme naturally to one-dimensional systems, based on a local characteristic field decomposition, and using the principles as in the scalar case to distribute the residuals in the characteristic fields.

3.1. One-dimensional scalar problems

We have the one-dimensional scalar steady state problem

$$f(u)_x = g(u,x). \tag{3.1}$$

We define the grid to be $\{x_i\}_{i=0,\ldots,N}$, grid function $\{u_i\}_{i=0,\ldots,N}$, the interval $I_{i+\frac{1}{2}} = [x_i, x_{i+1}]$, the control volume centered at x_i to be C_i (from the mid-point of the interval $I_{i-\frac{1}{2}}$ to the mid-point of the interval $I_{i+\frac{1}{2}}$), and the length of C_i is denoted by $|C_i|$.

The residual in the interval $I_{i+\frac{1}{2}}$ is define by

$$\Phi_{i+\frac{1}{2}} = \int_{x_i}^{x_{i+1}} (f(u)_x - g(u,x))\,\mathrm{d}x = f(u_{i+1}) - f(u_i) - \int_{x_i}^{x_{i+1}} g(u,x)\,\mathrm{d}x. \tag{3.2}$$

If we can reach the zero residual limit, i.e., if $\Phi_{i+\frac{1}{2}} = 0$ for all i, then the accuracy of the scheme is determined by the accuracy of the approximation to $\int_{x_i}^{x_{i+1}} g(u,x)\,\mathrm{d}x$. In our scheme, we use a fourth order central WENO integration, which is described in Section 2, to approximate the integral $\int_{x_i}^{x_{i+1}} g(u,x)\,\mathrm{d}x$ ($k = 3$, leading to a fifth order central WENO approximation to the integral in each cell and hence a fourth order approximation to the integral over the whole computational domain). Fourth order accuracy is therefore guaranteed at the zero residual limit.

Next, we start to distribute the residuals. In the interval $[x_i, x_{i+1}]$, the residual is $\Phi_{i+\frac{1}{2}}$, and it is to be distributed to the nodes x_i and x_{i+1}. For simplicity and with no ambiguity, we drop the subscript $i+\frac{1}{2}$ for the residuals. Here we denote the residual distributed to the point x_{i+1} and x_i as Φ^+ and Φ^-, respectively. We require $\Phi = \Phi^+ + \Phi^-$ for the conservation and require $|\Phi^\pm|/|\Phi|$ to be uniformly bounded (this is usually referred to as the residual property [1], which implies that when the zero residual limit $\Phi_{i+\frac{1}{2}} = 0$ is reached, the distributed residuals $\Phi^\pm$ are also zeros). To have an upwind scheme, one way to distribute the residual is the following:

$$\Phi^+ = \alpha\Phi, \quad \Phi^- = (1-\alpha)\Phi, \quad \alpha \in [0,1] \tag{3.3}$$

with α determined by

$$\alpha = \begin{cases} 1 & \text{if } \bar{\lambda} \geqslant \varepsilon, \\ 0 & \text{if } \bar{\lambda} \leqslant -\varepsilon, \\ r(\bar{\lambda}, \varepsilon), & \text{otherwise,} \end{cases}$$

where $\bar{\lambda} = f'(\bar{u})$, and $\bar{u}$ is the average state in the cell taken to be $\frac{1}{2}(u_i + u_{i+1})$. The function $r(\cdot,\cdot)$ is a continuously differentiable entropy correction function for the Roe scheme [15] which is given by

$$r(\lambda, \varepsilon) = \frac{1}{4\varepsilon^3}(\lambda+\varepsilon)^2(2\varepsilon - \lambda), \tag{3.4}$$

where ε is chosen accordingly in the problem.

Finally, the point value u_i is updated through sending the distributed residuals to the point x_i, as in a pseudo time-marching scheme, which can be written as a semi-discrete system

$$\frac{\mathrm{d}u_i}{\mathrm{d}t} + \frac{1}{|C_i|}\left(\Phi^+_{i-\frac{1}{2}} + \Phi^-_{i+\frac{1}{2}}\right) = 0. \tag{3.5}$$

In our numerical experiments, we use a third order TVD Runge–Kutta scheme [28] for the (pseudo) time discretization. Since the accuracy in time is irrelevant here, any stable time marching can be used, and strategies such as preconditioning and multigrid can be used to accelerate convergence towards steady state, but we do not pursue these approaches in this paper. Because of the residual property, namely the uniform boundedness of $|\Phi^\pm|/|\Phi|$, a zero residual limit $\Phi_{i+\frac{1}{2}} = 0$ is clearly also a steady state solution of (3.5). Conversely, a steady state solution of (3.5) may not imply a zero residual limit $\Phi_{i+\frac{1}{2}} = 0$ for all i. Our numerical experiments indicate that, near shocks, $\Phi_{i+\frac{1}{2}}$ may not be small even if the steady state solution of (3.5) is reached. Convergence towards weak solutions in this case would thus need to rely on a Lax–Wendroff type theorem stated and proved below, in the same spirit as that in [5].

Following the notations as above, we additionally denote $\Delta x_{i+\frac{1}{2}} = x_{i+1} - x_i$ and $\Delta x = \max_i \Delta x_i$, and define the function $u_{\Delta x}$ as a piecewise constant function where $u_{\Delta x}(x) = u_i$, $x \in C_i$.

As defined in Eq. (3.2), the residual is approximated by

$$\Phi_{i+\frac{1}{2}} = f(u_{i+1}) - f(u_i) - \mathscr{R}(g(u_{\Delta x}, x), I_{i+\frac{1}{2}}), \tag{3.6}$$

where $\mathscr{R}\left(g(u_{\Delta x}, x), I_{i+\frac{1}{2}}\right)$ is an approximation of $\int_{I_{i+\frac{1}{2}}} g(u,x)\,\mathrm{d}x$, which can be written as a linear combination of the point values of g. The distributed residuals, as defined in Eq. (3.3), are $\Phi^\pm_{i+\frac{1}{2}}$, with the conservation property,

$$\Phi_{i+\frac{1}{2}} = \Phi^+_{i+\frac{1}{2}} + \Phi^-_{i+\frac{1}{2}} \tag{3.7}$$

and the residual property

$$\frac{\left|\Phi^\pm_{i+\frac{1}{2}}\right|}{\left|\Phi_{i+\frac{1}{2}}\right|} \leqslant C, \tag{3.8}$$

where here and below C with or without subscriptions denotes constants independent of the mesh sizes. Equipped with the above properties, we have the following theorem.

Theorem 3.1. *Assume that the flux function f in Eq. (3.1) is Lipschitz continuous, and the source term $g(u,x)$ is continuous in both arguments. If $u_{\Delta x}$ is a steady state solution of Eq. (3.5) satisfying Eqs. (3.6)–(3.8), and if there is a function u with bounded total variation such that*

$$u_{\Delta x} \to u \quad \text{in } L^1(\mathbb{R}), \quad \text{as } \Delta x \to 0$$

and

$$\sup_{\Delta x} \sup_{x} |u_{\Delta x}(x)| \leqslant C_1$$

then u is a weak solution to Eq. (3.1).

Proof. At steady state of the scheme, $\Phi^+_{i-\frac{1}{2}} + \Phi^-_{i+\frac{1}{2}} = 0$ for all i. Let $\varphi \in C_0^\infty(\mathbb{R})$ be a test function, and denote $\varphi_i = \varphi(x_i)$. We have,

$$\begin{aligned} 0 &= \sum_i \left(\Phi^+_{i-\frac{1}{2}} + \Phi^-_{i+\frac{1}{2}}\right)\varphi_i = \sum_i \Phi^+_{i-\frac{1}{2}}\varphi_i + \Phi^-_{i+\frac{1}{2}}(\varphi_{i+1} - \varphi_{i+1} + \varphi_i) \\ &= \sum_i \left(\Phi^+_{i-\frac{1}{2}} + \Phi^-_{i-\frac{1}{2}}\right)\varphi_i - \sum_i \Phi^-_{i-\frac{1}{2}}(\varphi_i - \varphi_{i-1}) = \sum_i \Phi_{i-\frac{1}{2}}\varphi_i - \sum_i \Phi^-_{i-\frac{1}{2}}(\varphi_i - \varphi_{i-1}) = \mathrm{I} + \mathrm{II}. \end{aligned}$$

We look at the first summation term,

$$\begin{aligned} \mathrm{I} &= \sum_i \Phi_{i-\frac{1}{2}}\varphi_i = \sum_i \left(f(u_i) - f(u_{i-1}) - \mathscr{R}\left(g(u_{\Delta x}, x), I_{i-\frac{1}{2}}\right)\right)\varphi_i \\ &= \sum_i (f(u_i) - f(u_{i-1}))\varphi_i - \sum_i \mathscr{R}\left(g(u_{\Delta x}, x), I_{i-\frac{1}{2}}\right)\varphi_i \\ &= -\sum_i f(u_i)\frac{(\varphi_{i+1} - \varphi_i)}{\Delta x_{i+\frac{1}{2}}}\Delta x_{i+\frac{1}{2}} - \sum_i \mathscr{R}\left(g(u_{\Delta x}, x), I_{i-\frac{1}{2}}\right)\varphi_i. \end{aligned}$$

Note that

$$-\sum_i f(u_i)\frac{(\varphi_{i+1} - \varphi_i)}{\Delta x_{i+\frac{1}{2}}}\Delta x_{i+\frac{1}{2}} \to -\int f(u)\varphi_x \,\mathrm{d}x \quad \text{as } \Delta x \to 0$$

and

$$\sum_i \mathscr{R}(g(u_{\Delta x}, x), I_{i-\frac{1}{2}})\varphi_i \to \int g(u,x)\varphi \,\mathrm{d}x \quad \text{as } \Delta x \to 0.$$

Therefore, $\mathrm{I} \to -\int f(u)\varphi_x \,\mathrm{d}x - \int g(u,x)\varphi \,\mathrm{d}x$ as $\Delta x \to 0$.

Next, we estimate the second term II

$$\begin{aligned} |\mathrm{II}| &= \left|\sum_i \Phi^-_{i-\frac{1}{2}}(\varphi_i - \varphi_{i-1})\right| \leqslant \sum_i \left|\Phi^-_{i-\frac{1}{2}}\right||\varphi_i - \varphi_{i-1}| \leqslant C\sum_i \left|\Phi_{i-\frac{1}{2}}\right||\varphi_i - \varphi_{i-1}| \\ &\leqslant C\sum_i |f(u_i) - f(u_{i-1})||\varphi_i - \varphi_{i-1}| + C\sum_i \left|\mathscr{R}\left(g(u_{\Delta x}, x), I_{i-\frac{1}{2}}\right)\right|\frac{|\varphi_i - \varphi_{i-1}|}{\Delta x_{i-\frac{1}{2}}}\Delta x_{i-\frac{1}{2}} \\ &\leqslant C_2\sum_i |u_i - u_{i-1}|\Delta x + C_2\Delta x\sum_i \left|\mathscr{R}\left(g(u_{\Delta x}, x), I_{i-\frac{1}{2}}\right)\right|\frac{|\varphi_i - \varphi_{i-1}|}{\Delta x_{i-\frac{1}{2}}}. \end{aligned}$$

The second term above without the Δx factor converges to $C_2\int |g(u,x)\varphi_x| \,\mathrm{d}x$ and hence the second term itself is $\mathrm{O}(\Delta x)$. As for the first term,

$$\sum_i |u_i - u_{i-1}|\Delta x \leqslant \sum_i |u_i - u(x_i)|\Delta x + \sum_i |u(x_i) - u(x_{i-1})|\Delta x + \sum_i |u(x_{i-1}) - u_{i-1}|\Delta x.$$

By the L^1 convergence of the scheme and the fact that $u(x)$ has bounded total variation, $|\mathrm{II}| \to 0$ as $\Delta x \to 0$, and we can conclude that

$$-\int f(u)\varphi_x \,\mathrm{d}x - \int g(u,x)\varphi \,\mathrm{d}x = 0,$$

namely, u is a weak solution to Eq. (3.1). □

We now summarize the procedure of the high order RD finite difference WENO scheme for one-dimensional scalar problems:

1. Compute the residuals defined in Eq. (3.2) using WENO integration with a proper accuracy.
2. Distribute the residuals according to the upwinding principle, which is defined in Eq. (3.3).
3. Update the point values through sending the residuals and forward in pseudo time (3.5) by a TVD Runge–Kutta time discretization until the steady state is reached.

3.2. One-dimensional systems

Consider a one-dimensional steady state system (3.1) where u, $f(u)$ and $g(u)$ are vector-valued functions in $\mathbb{R}^m$. For hyperbolic systems, we assume that the Jacobian $f'(u)$ can be written as $L\Lambda R$, where Λ is a diagonal matrix with real eigenvalues on the diagonal, and L and R are matrices of left and right eigenvectors of $f'(u)$, respectively.

The grid, grid function and the control volumes are denoted as in Section 3.1. The residual in the interval $[x_i, x_{i+1}]$ is again defined by (3.2). As before, the accuracy of the scheme is determined by the accuracy of the approximation to $\int_{x_i}^{x_{i+1}} g(u,x)\,\mathrm{d}x$, which is again obtained by a fourth order central WENO integration.

In order to distribute the residual $\Phi_{i+\frac{1}{2}}$, we use a local characteristic decomposition in the interval $[x_i, x_{i+1}]$. First, we compute an average state $\bar{u}$ between u_i and u_{i+1}, using either the simple arithmetic mean or a Roe's average [22], and denote $\bar{L}$ and $\bar{R}$ to be the matrices with left and right eigenvectors L and R evaluated at the average state, and $\bar{\lambda}_k$ the corresponding kth eigenvalue. In the following, for simplicity of the notation and with no ambiguity, we drop the subscript $i+\frac{1}{2}$ in the residuals. We project the residual Φ to the characteristic fields, namely, $\Psi = \bar{R}\Phi$. The residual Ψ is to be distributed to the two endpoints x_i and x_{i+1}, and we denote the residual sent to x_{i+1} and x_i by Ψ^+ and Ψ^-, respectively, with $\Psi = \Psi^+ + \Psi^-$. Those residuals are defined by

$$\Psi^+ = \Sigma\Psi, \quad \Psi^- = (\mathrm{I} - \Sigma)\Psi, \tag{3.9}$$

where I is the identity matrix and Σ is a diagonal matrix with the kth diagonal component

$$\Sigma_{kk} = \begin{cases} 1 & \text{if } \bar{\lambda}_k \geqslant \varepsilon, \\ 0 & \text{if } \bar{\lambda}_k \leqslant -\varepsilon, \\ r(\bar{\lambda}_k, \varepsilon), & \text{otherwise} \end{cases}$$

with the function $r(\cdot,\cdot)$ defined by (3.4) and ε chosen accordingly in the problem.

Next, we project the distributed residuals back to the physical space, and denote Φ^+ and Φ^- to be the residuals in the physical space which are sent to the points x_{i+1} and x_i, respectively,

$$\Phi^+ = \bar{L}\Psi^+, \quad \Phi^- = \bar{L}\Psi^-. \tag{3.10}$$

Finally, as in the scalar case, the point value u_i can be updated in the pseudo time-marching semi-discrete scheme (3.5), which is again discretized by a third order TVD Runge–Kutta scheme in our numerical experiments until steady state is reached.

We now summarize the procedure of the high order RD finite difference WENO scheme for one-dimensional steady state systems:

1. Compute the residuals defined in Eq. (3.2) using WENO integration with a proper accuracy.
2. Project the residuals to local characteristic fields.

3. Distribute the residuals according to the upwinding principle in characteristic fields, which is defined in Eq. (3.9).
4. Project the distributed residuals in characteristic fields back to the physical space as in (3.10).
5. Update the point values through sending the residuals in the physical space and forward in pseudo time (3.5) by a TVD Runge–Kutta time discretization until the steady state is reached.

4. High order RD finite difference WENO schemes in two dimension

In this section, we design a high order RD finite difference WENO scheme for two-dimensional steady state problems on non-smooth curvilinear meshes. To be more precise, we restrict our attention to such curvilinear meshes which can be smoothly mapped to non-smooth Cartesian meshes. We will use Cartesian meshes as examples to describe our algorithm. The numerical experiments in next section will contain both Cartesian meshes and a special class of quadrilateral meshes consisting of parallelograms. The procedure on general curvilinear meshes is similar. In Section 4.1, we define the residuals from the integral form, as in Eq. (1.2), and then describe the distribution mechanism. In Section 4.2, we extend the scheme to two-dimensional systems, based on a local characteristic field decomposition, and distributing the residuals in characteristic fields dimension-by-dimension.

4.1. Two-dimensional scalar problems

We have the two-dimensional scalar steady state problem

$$f(u)_x + g(u)_y = h(u,x,y). \tag{4.1}$$

We define the grid to be $\{(x_i,y_j)\}$, grid function $\{u_{ij}\}$, the cells $I_{i+\frac{1}{2},j+\frac{1}{2}} = [x_i, x_{i+1}] \times [y_j, y_{j+1}]$, the control volume centered at (x_i,y_j) to be C_{ij} (formed by connecting the centers of the four cells sharing (x_i,y_j) as a common node), and the area of C_{ij} is denoted by $|C_{ij}|$.

The residual in the cell $I_{i+\frac{1}{2},j+\frac{1}{2}}$ is defined by

$$\begin{aligned}\Phi_{i+\frac{1}{2},j+\frac{1}{2}} &= \int_{y_j}^{y_{j+1}} \int_{x_i}^{x_{i+1}} (f(u)_x + g(u)_y - h(u,x,y))\,\mathrm{d}x\,\mathrm{d}y \\ &= \int_{y_j}^{y_{j+1}} (f(u(x_{i+1},y)) - f(u(x_i,y)))\,\mathrm{d}y + \int_{x_i}^{x_{i+1}} \big(g(u(x,y_{j+1})) - g(u(x,y_j))\big)\,\mathrm{d}x \\ &\quad - \int_{y_j}^{y_{j+1}} \int_{x_i}^{x_{i+1}} h(u(x,y),x,y)\,\mathrm{d}x\,\mathrm{d}y.\end{aligned} \tag{4.2}$$

If we reach the zero residual limit, i.e., if $\Phi_{i+\frac{1}{2},j+\frac{1}{2}} = 0$ for all i and j, the accuracy of the scheme is determined by the accuracy of the approximations to the integrations of the fluxes and the source term.

To approximate the integration of the fluxes, which are one-dimensional integrals, we use a fourth order central WENO integration described in Section 2. As for the source term $\int_{y_j}^{y_{j+1}} \int_{x_i}^{x_{i+1}} h(u,x,y)\,\mathrm{d}x\,\mathrm{d}y$, we can approximate it in a dimension-by-dimension fashion, which is explained as follows. First, we define

$$H_{j+\frac{1}{2}}(x) = \int_{y_j}^{y_{j+1}} h(u(x,y),x,y)\,\mathrm{d}y$$

and hence

$$\int_{y_j}^{y_{j+1}} \int_{x_i}^{x_{i+1}} h(u,x,y)\,\mathrm{d}x\,\mathrm{d}y = \int_{x_i}^{x_{i+1}} H_{j+\frac{1}{2}}(x)\,\mathrm{d}x.$$

The integral $\int_{x_i}^{x_{i+1}} H_{j+\frac{1}{2}}(x)\,\mathrm{d}x$ can be approximated by a fourth order WENO integration in the x-direction, using $\left\{H_{j+\frac{1}{2}}(x_{i+k})\right\}_{k=-1,\ldots,2}$. By the definition of $H_{j+\frac{1}{2}}(x)$, $H_{j+\frac{1}{2}}(x_{i+k})$ can again be approximated by a fourth order

WENO integration in the y-direction, using $\{h(u_{i+k,j+l}, x_{i+k}, y_{j+l})\}_{l=-1,\ldots,2}$. Therefore, the integration of the source term can be approximated dimension-by-dimension, and the fourth order accuracy is obtained at the zero residual limit.

Next, we start to distribute the residuals. In the cell $I_{i+\frac{1}{2},j+\frac{1}{2}} = [x_i, x_{i+1}] \times [y_j, y_{j+1}]$, the residual is $\Phi_{i+\frac{1}{2},j+\frac{1}{2}}$, and it is to be distributed to the vertices of the cell, which are defined to be $M_1 = (x_{i+1}, y_{j+1})$, $M_2 = (x_{i+1}, y_j)$, $M_3 = (x_i, y_{j+1})$ and $M_4 = (x_i, y_j)$. Here, we define the residuals sent to the vertices M_k as $\Phi^k_{i+\frac{1}{2},j+\frac{1}{2}}$ for $k = 1, \ldots, 4$. For simplicity and without ambiguity, we drop the subscript $\left(i+\frac{1}{2}, j+\frac{1}{2}\right)$ in the notations. For conservation and the residual property, we require $\Phi = \sum_{k=1}^4 \Phi^k$ and $|\Phi^k|/|\Phi|$ to be uniformly bounded.

To have an upwind scheme, one way to distribute the residual is the following:

$$\Phi^1 = \alpha\beta\Phi, \quad \Phi^2 = \alpha(1-\beta)\Phi, \quad \Phi^3 = (1-\alpha)\beta\Phi, \quad \Phi^4 = (1-\alpha)(1-\beta)\Phi, \qquad \alpha, \beta \in [0,1] \tag{4.3}$$

and α, the coefficient for upwinding in the x-direction, is given by

$$\alpha = \begin{cases} 1 & \text{if } \bar{\lambda}_x \geqslant \varepsilon, \\ 0 & \text{if } \bar{\lambda}_x \leqslant -\varepsilon, \\ r(\bar{\lambda}, \varepsilon), & \text{otherwise,} \end{cases}$$

where $\bar{\lambda}_x = f'(\bar{u})$, and $\bar{u}$ is an average state in the cell defined by $\frac{1}{4}(u_{i,j} + u_{i+1,j} + u_{i+1,j+1} + u_{i,j+1})$. Similarly, β, the coefficient for upwinding in the y-direction, is given by

$$\beta = \begin{cases} 1 & \text{if } \bar{\lambda}_y \geqslant \varepsilon, \\ 0 & \text{if } \bar{\lambda}_y \leqslant -\varepsilon, \\ r(\bar{\lambda}, \varepsilon), & \text{otherwise,} \end{cases}$$

where $\bar{\lambda}_y = g'(\bar{u})$. $r(\cdot,\cdot)$ is given in Eq. (3.4) and ε is chosen accordingly in the problem.

Our numerical experience indicates that extra dissipation is necessary near shocks for the pseudo time marching towards steady state to proceed in a stable fashion. We therefore add an additional dissipation residual Φ^k_{diss} to each of Φ^k, only around the shocks. The dissipation residuals are defined as the following:

$$\begin{aligned}
\Phi^1_{\text{diss}} &= \frac{\delta}{2}\Delta^3\left(\frac{u_{i+1,j+1} - u_{i,j+1}}{\Delta x_{i+\frac{1}{2}}} + \frac{u_{i+1,j+1} - u_{i+1,j}}{\Delta y_{j+\frac{1}{2}}}\right), \\
\Phi^2_{\text{diss}} &= \frac{\delta}{2}\Delta^3\left(\frac{u_{i+1,j} - u_{i,j}}{\Delta x_{i+\frac{1}{2}}} + \frac{u_{i+1,j} - u_{i+1,j+1}}{\Delta y_{j+\frac{1}{2}}}\right), \\
\Phi^3_{\text{diss}} &= \frac{\delta}{2}\Delta^3\left(\frac{u_{i,j+1} - u_{i+1,j+1}}{\Delta x_{i+\frac{1}{2}}} + \frac{u_{i,j+1} - u_{i,j}}{\Delta y_{j+\frac{1}{2}}}\right), \\
\Phi^4_{\text{diss}} &= \frac{\delta}{2}\Delta^3\left(\frac{u_{i,j} - u_{i+1,j}}{\Delta x_{i+\frac{1}{2}}} + \frac{u_{i,j} - u_{i,j+1}}{\Delta y_{j+\frac{1}{2}}}\right),
\end{aligned} \tag{4.4}$$

where $\Delta = \max\left(\Delta x_{i+\frac{1}{2}}, \Delta y_{j+\frac{1}{2}}\right)$ and the dissipation coefficient δ is chosen accordingly in the problem.

Finally, we define the distributed residuals by $\tilde{\Phi}^k = \Phi^k + \theta\Phi^k_{\text{diss}}, k = 1, \ldots, 4$, where θ is a discontinuity indicator defined by $\theta = \max(\theta_x, \theta_y)$, with the one-dimensional discontinuity indicators θ_x and θ_y for the x and y directions given as in [33]; θ_x is defined by $\theta_x = \frac{\beta}{\beta+\gamma}$ with

$$\alpha_i = |u_{i-1,j} - u_{i,j}|^2 + \varepsilon, \quad \beta = \left(\frac{\alpha_i}{\alpha_{i-1}} + \frac{\alpha_{i+1}}{\alpha_{i+2}}\right)^2, \quad \gamma = \frac{|u_{\max} - u_{\min}|^2}{\alpha_i} \tag{4.5}$$

and θ_y is defined similarly, but in the y-direction. A similar indicator with a wider stencil

$$\beta = \left(\frac{\alpha_{i-2}}{\alpha_{i-3}} + \frac{\alpha_{i-1}}{\alpha_{i-2}} + \frac{\alpha_i}{\alpha_{i-1}} + \frac{\alpha_{i+1}}{\alpha_{i+2}} + \frac{\alpha_{i+2}}{\alpha_{i+3}} + \frac{\alpha_{i+3}}{\alpha_{i+4}}\right)^2, \quad \gamma = \frac{|u_{\max} - u_{\min}|^2}{\alpha_{i-1} + \alpha_i + \alpha_{i+1} + \alpha_{i+2}}$$

with the same α_i as that defined in (4.5), is used for two-dimensional systems. Here ε is a small positive number taken as 10^{-6} in our numerical experiments, and $u_{\max}$ and $u_{\min}$ are the maximum and minimum values of u_{ij} for all grid points. Clearly, $0 \leqslant \theta \leqslant 1$. Near a strong discontinuity, $\gamma \ll \beta$, θ is close to 1. However, in smooth regions, $\theta = O(\Delta^2)$, hence fourth order accuracy is maintained in smooth regions. This dissipation mechanism works well for our numerical experiments, but it may not be the optimal approach as it has an adjustable coefficient δ, whose choice for optimal performance seems to be problem dependent. Other dissipation mechanisms, such as the one adopted by Abgrall in [2], will be explored in the future.

The point value u_{ij} is then updated through sending the distributed residuals to the point (x_i, y_j), as in a pseudo time-marching scheme, which can be written as a semi-discrete system

$$\frac{\mathrm{d}u_{ij}}{\mathrm{d}t} + \frac{1}{|C_{ij}|}\left(\tilde{\Phi}^4_{i+\frac{1}{2},j+\frac{1}{2}} + \tilde{\Phi}^3_{i+\frac{1}{2},j-\frac{1}{2}} + \tilde{\Phi}^2_{i-\frac{1}{2},j+\frac{1}{2}} + \tilde{\Phi}^1_{i-\frac{1}{2},j-\frac{1}{2}}\right) = 0. \tag{4.6}$$

We again use a third order TVD Runge–Kutta scheme for the pseudo time discretization. As in the one-dimensional case, a steady state of Eq. (4.6) may not imply a zero residual $\Phi_{i+\frac{1}{2},j+\frac{1}{2}} = 0$ for all i,j, and $\Phi_{i+\frac{1}{2},j+\frac{1}{2}}$ may not be small around the shocks even if the steady state solution of Eq. (4.6) is reached. Moreover, we may lose the strict residual property after adding dissipation residuals, but note that conservation is still preserved after adding the dissipation since $\sum_{k=1}^4 \Phi^k_{\mathrm{diss}} = 0$. In addition, the residual property is maintained in smooth regions. It might be possible to improve upon the design of these dissipation residuals to remove their negative effect on local residual property, along the lines of [1,8]. This will be investigated in the future. Convergence toward weak solutions in this case rely on a Lax–Wendroff type theorem, and the proof is similar to that of the one-dimensional case, but is more technical, hence we leave that to Appendix A.

We now summarize the procedure of the high order RD finite difference WENO scheme for two-dimensional scalar steady state problems:

1. Compute the residuals (4.2) using WENO integration with a proper accuracy.
2. Distribute the residuals according to the upwinding principle, which is defined in Eq. (4.3).
3. Revise the residuals by adding a dissipation residual (4.4).
4. Update the point values through sending the residuals and forward in pseudo time (4.6) by a TVD Runge–Kutta time discretization until the steady state is reached.

4.2. Two-dimensional systems

Consider a two-dimensional steady state system (4.1) where u, $f(u)$, $g(u)$ and $h(u,x,y)$ are vector-valued functions in $\mathbb{R}^m$. For hyperbolic systems, we assume that any real linear combination of the Jacobians $\xi_1 f'(u) + \xi_2 g'(u)$ is diagonalizable with real eigenvalues. In particular, we assume $f'(u)$ and $g'(u)$ can be written as $L_x \Lambda_x R_x$ and $L_y \Lambda_y R_y$, respectively, where Λ_x and Λ_y are diagonal matrices with real eigenvalues on the diagonal, and L_x, R_x and L_y, R_y are matrices of left and right eigenvectors for the corresponding Jacobians.

The grid, grid function and the control volumes are denoted as in Section 4.1. The residual in the cell $I_{i+\frac{1}{2},j+\frac{1}{2}} = [x_i, x_{i+1}] \times [y_j, y_{j+1}]$ is still defined by (4.2). As before, if we reach the zero residual limit of the scheme, the accuracy of the scheme is determined by the accuracy of the approximations to the integrations of the fluxes and the source term. We again use a fourth order central WENO integration described in Section 2. For simplicity and without ambiguity, we drop the subscript $\left(i+\frac{1}{2}, j+\frac{1}{2}\right)$ in the residuals in the following.

We would distribute the residual Φ to the four vertices $\{M_k\}_{k=1,\ldots,4}$, defined in Section 4.1, and the corresponding residuals are still denoted by $\{\Phi^k\}_{k=1,\ldots,4}$, where $\Phi^k \in \mathbb{R}^m$. We also require $\Phi = \sum_{k=1}^4 \Phi^k$ and the residual property that $|\Phi^k|/|\Phi|$ should stay uniformly bounded. Here we consider a dimension-by-dimension procedure, coupled with a local characteristic field decomposition. First, we compute an average state $\bar{u}$ in $I_{i+\frac{1}{2},j+\frac{1}{2}}$, using either the simple arithmetic mean or a Roe's average [22], and denote $\bar{L}_x$ and $\bar{R}_x$ as the matrices with left and right eigenvectors L_x and R_x of $f'(u)$ evaluated at the average state, and $\bar{\lambda}^k_x$ the corresponding eigenvalues; $\bar{L}_y$, $\bar{R}_y$ and $\bar{\lambda}^k_y$ are defined similarly but associated with L_y, R_y and Λ_y of $g'(u)$.

We first consider the x-direction and project the residual Φ to the x-characteristic fields: $\Psi = \bar{R}_x \Phi$. The residual Ψ is to be split into two parts in the x-direction: one is Ψ^+, which is sent to the side x_{i+1}; the other is Ψ^-, sent to the side x_i, and $\Psi = \Psi^+ + \Psi^-$. $\Psi^\pm$ are defined by

$$\Psi^+ = \Sigma\Psi, \quad \Psi^- = (\mathrm{I} - \Sigma)\Psi, \tag{4.7}$$

where I is the identity matrix and Σ is a diagonal matrix with the kth diagonal component

$$\Sigma_{kk} = \begin{cases} 1 & \text{if } \bar{\lambda}_x^k \geqslant \varepsilon, \\ 0 & \text{if } \bar{\lambda}_x^k \leqslant -\varepsilon, \\ r(\bar{\lambda}_x^k, \varepsilon) & \text{otherwise} \end{cases}$$

with the function $r(\cdot,\cdot)$ defined by (3.4) and ε chosen accordingly in the problem. Then we project $\Psi^\pm$ back to the physical space to obtain $\hat{\Phi}^\pm$

$$\hat{\Phi}^+ = \bar{L}_x \Psi^+, \quad \hat{\Phi}^- = \bar{L}_x \Psi^-.$$

Next, we consider the y-direction, and we would distribute the two parts $\hat{\Phi}^\pm$ in the y-direction. We first project $\hat{\Phi}^\pm$ to the y-characteristic fields to obtain $\Pi^\pm$

$$\Pi^+ = \bar{R}_y \hat{\Phi}^+, \quad \Pi^- = \bar{R}_y \hat{\Phi}^-.$$

Then we distribute $\Pi^\pm$ in the y-characteristic fields according to upwinding and the residual property as follows:

$$\bar{\Psi}^1 = \Gamma\Pi^+, \quad \bar{\Psi}^2 = (\mathrm{I} - \Gamma)\Pi^+, \quad \bar{\Psi}^3 = \Gamma\Pi^-, \quad \bar{\Psi}^4 = (\mathrm{I} - \Gamma)\Pi^-, \tag{4.8}$$

where I is the identity matrix and Γ is a diagonal matrix with the kth diagonal component

$$\Gamma_{kk} = \begin{cases} 1 & \text{if } \bar{\lambda}_y^k \geqslant \varepsilon, \\ 0 & \text{if } \bar{\lambda}_y^k \leqslant -\varepsilon, \\ r(\bar{\lambda}_y^k, \varepsilon), & \text{otherwise.} \end{cases}$$

Finally, we project the distributed residuals back to the physical space

$$\Phi^k = \bar{L}_y \bar{\Psi}^k, \quad k = 1, \ldots, 4.$$

As in the scalar case, we add a dissipation residual Φ^k_{diss} to each of Φ^k around the shocks. The dissipation residuals are defined in Eq. (4.4). We define the distributed residuals by $\tilde{\Phi}^k = \Phi^k + \theta\Phi^k_{\text{diss}}$, $k = 1, \ldots, 4$, where θ is the discontinuity indicator given in Section 4.1.

The point value u_{ij} is then updated through sending the distributed residuals to the point (x_i, y_j), as in a pseudo time-marching scheme, which can be written as the semi-discrete system (4.6). We again use a third order TVD Runge–Kutta scheme for the pseudo time discretization.

We now summarize the procedure of the high order RD finite difference WENO scheme for two-dimensional steady state systems:

1. Compute the residuals defined in Eq. (4.2) using WENO integration with a proper accuracy.
2. Project the residuals to the local x-characteristic fields.
3. Distribute the residuals in the x-direction according to the upwinding principle, which is defined in Eq. (4.7), and transform the two parts of residuals back to the physical space.
4. Project the residuals to the local y-characteristic fields.
5. Distribute the residuals in the y-direction, according to Eq. (4.8), and transform the four distributed residuals back to the physical space.
6. Revise the residuals by adding a dissipation residual.
7. Update the point values through sending the residuals and forward in pseudo time (4.6) by a TVD Runge–Kutta time discretization until the steady state is reached.

As before, conservation is still preserved after adding the dissipation since $\sum_{k=1}^{4} \Phi_{\text{diss}}^{k} = 0$. In addition, the residual property is maintained in smooth regions.

In our numerical tests in following section, there are several examples (Examples 5.4.1, 5.4.3 and 5.4.4) in which the L^1 residue can only be reduced to around 10^{-4}–10^{-6} and then stagnates at that level. This might be related to the boundary conditions or lack of suitable numerical dissipation in certain regimes. More study is needed to address this issue.

5. Numerical results

In this section, we provide numerical experimental results to demonstrate the behavior of our schemes. Pseudo time discretization towards steady state is by the third order TVD Runge–Kutta method in all numerical simulations. In Sections 5.1 and 5.2, for one-dimensional problems, the parameter ε in (3.4) for Roe's entropy correction is taken as 0; and in Sections 5.3 and 5.4, for two-dimensional problems, ε is taken as 0.1 unless otherwise stated.

5.1. One-dimensional scalar problems

In this section, numerical steady state is obtained with L^1 residue reduced to the round-off level.

Example 5.1.1. We solve the steady state solution of the one-dimensional Burgers equation with a source term

$$u_t + \left(\frac{u^2}{2}\right)_x = \sin x \cos x \tag{5.1}$$

with the initial condition

$$u(x,0) = \beta \sin x \tag{5.2}$$

and the boundary condition $u(0,t) = u(\pi,t) = 0$. This problem was studied in [24] as an example of multiple steady state solutions for characteristic initial value problems. Here we take $\beta = 2$, which gives a smooth steady state solution $u(x,\infty) = \sin x$. We test our scheme on both uniform meshes and non-smooth meshes which are obtained by randomly perturbing each node of the uniform mesh up to 20% of the mesh sizes. The numerical results are shown in Table 1. We can see clearly that fourth order accuracy is achieved and the magnitudes of the errors are comparable for both uniform and non-uniform, non-smooth meshes.

Example 5.1.2. We solve the Burgers equation (5.1) and take $\beta = 0.5$ in (5.2) as the initial condition. This problem has a solution with a shock, located at $\pi - \arcsin\sqrt{1-\beta^2} \approx 2.0944$. The numerical solution on a non-smooth mesh which is 20% randomly perturbed is shown in Fig. 1. We can see that the numerical shock is at the correct location and is resolved well.

Table 1
Errors and numerical orders of accuracy of the fourth order RD finite difference WENO scheme for Example 5.1.1 on non-smooth and uniform meshes with N cells

N	Non-smooth mesh				Uniform mesh			
	L^1 error	Order	L^∞ error	Order	L^1 error	Order	L^∞ error	Order
20	7.02E − 05	–	1.37E − 04	–	6.52E − 05	–	1.01E − 04	–
40	3.89E − 06	4.17	5.72E − 06	4.58	3.30E − 06	4.30	5.18E − 06	4.29
80	2.02E − 07	4.27	3.19E − 07	4.16	1.91E − 07	4.11	3.00E − 07	4.11
160	1.29E − 08	3.97	1.97E − 08	4.02	1.17E − 08	4.03	1.83E − 08	4.03
320	7.82E − 10	4.04	1.22E − 09	4.01	7.24E − 10	4.01	1.14E − 09	4.01
640	4.83E − 11	4.02	7.58E − 11	4.01	4.52E − 11	4.00	7.10E − 11	4.00

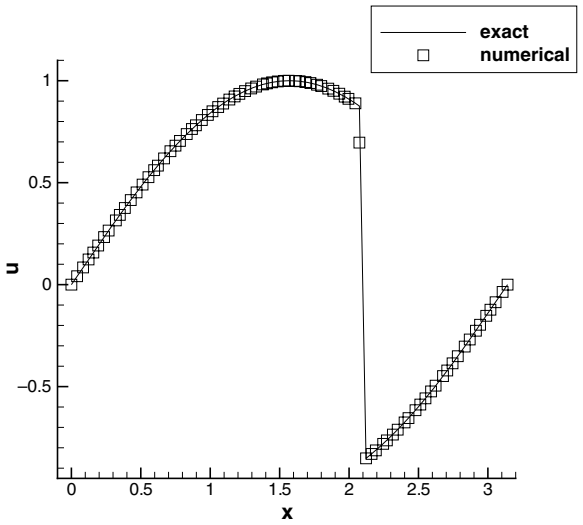

Fig. 1. The numerical solution (symbols) versus the exact solution (solid line) for Example 5.1.2. Non-smooth mesh with 80 cells.

Example 5.1.3. We consider the steady state solutions of the Burgers equation with a different source term:

$$u_t + \left(\frac{u^2}{2}\right)_x = -\pi \cos(\pi x) u, \quad x \in [0,1] \tag{5.3}$$

equipped with the boundary condition $u(0,t) = 1$ and $u(1,t) = -0.1$. This problem has two steady state solutions with shocks:

$$u(x,\infty) = \begin{cases} u^+ = 1 - \sin(\pi x) & \text{if } 0 \leqslant x < x_s, \\ u^- = -0.1 - \sin(\pi x) & \text{if } x_s \leqslant x < 1, \end{cases}$$

where $x_s = 0.1486$ or $x_s = 0.8514$. Both solutions satisfy the Rankine–Hugoniot jump condition and the entropy conditions, but only the one with the shock at 0.1486 is stable for small perturbation. This problem was studied in [13] as an example of multiple steady states for one-dimensional transonic flows. This case is tested to demonstrate that starting with a reasonable perturbation of the stable steady state, the numerical solution converges to the stable one.

The initial condition is given by

$$u(x,0) = \begin{cases} 1 & \text{if } 0 \leqslant x < 0.5, \\ -0.1 & \text{if } 0.5 \leqslant x < 1, \end{cases}$$

where the initial jump is located in the middle of the positions of the shocks in the two admissible steady state solutions. We test our scheme on a non-smooth mesh which is 20% perturbed from the uniform one. The numerical result and the exact solution are displayed in Fig. 2. We can see the correct shock location and good resolution of the shock.

5.2. One-dimensional systems

In this section, numerical steady state is obtained with L^1 residue reduced to the round-off level.

Example 5.2.1. We solve the steady state solutions of the one-dimensional shallow water equation

$$\begin{pmatrix} h \\ hu \end{pmatrix}_t + \begin{pmatrix} hu \\ hu^2 + \frac{1}{2}gh^2 \end{pmatrix}_x = \begin{pmatrix} 0 \\ -ghb_x \end{pmatrix}, \tag{5.4}$$

where h denotes the water height, u is the velocity of the fluid, $b(x)$ represents the bottom topography and g is the gravitational constant.

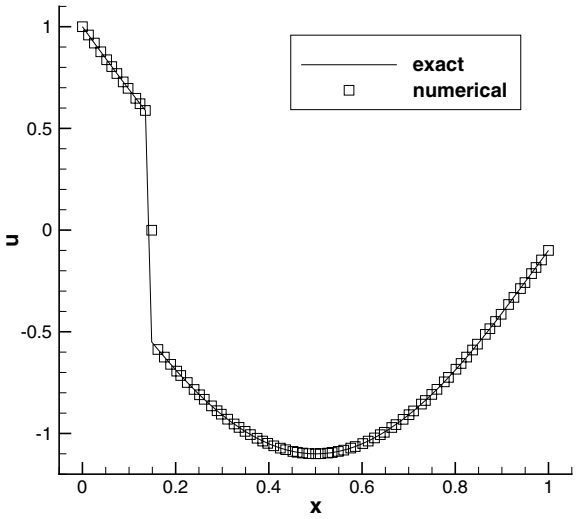

Fig. 2. The stable entropy solution (solid line) and the numerical solution (symbols) for Example 5.1.3. Non-smooth mesh with 80 cells.

Starting from a stationary initial condition, which itself is a steady state solution, we can check the order of accuracy. The smooth bottom topography is given by

$$b(x) = 5e^{-\frac{2}{5}(x-5)^2}, \quad x \in [0, 10].$$

The initial condition is the stationary solution

$$h + b = 10, \quad hu = 0$$

and the exact steady state solution is imposed as the boundary condition.

We test our scheme on uniform meshes as well as on non-smooth meshes which are 20% perturbed form the uniform ones. The numerical results are shown in Table 2. We can clearly see the order of accuracy and the errors on these two types of meshes are comparable.

Example 5.2.2. We test our scheme on the steady state solution of the one-dimensional nozzle flow problem

$$\begin{pmatrix} \rho \\ \rho u \\ E \end{pmatrix}_t + \begin{pmatrix} \rho u \\ \rho u^2 + p \\ u(E+p) \end{pmatrix}_x = -\frac{a'(x)}{a(x)} \begin{pmatrix} \rho u \\ \rho^2 u^2/\rho \\ u(E+p) \end{pmatrix}, \quad x \in [0, 1], \tag{5.5}$$

where ρ denotes the density, u is the velocity of the fluid, E is the total energy, γ is the gas constant, which is taken as 1.4, $p = (\gamma - 1)\left(E - \frac{1}{2}\rho u^2\right)$ is the pressure, and $a(x)$ represents the area of the cross-section of the nozzle.

Table 2
Errors and numerical orders of accuracy for the water height h of the fourth order RD finite difference WENO scheme for Example 5.2.1 on non-smooth and uniform meshes with N cells

N	Non-smooth mesh				Uniform mesh			
	L^1 error	Order	L^∞ error	Order	L^1 error	Order	L^∞ error	Order
20	4.55E − 03	–	1.67E − 02	–	5.29E − 03	–	1.65E − 02	–
40	3.83E − 04	3.57	9.61E − 04	4.12	2.71E − 04	4.29	8.81E − 04	4.23
80	1.52E − 05	4.66	4.23E − 05	4.50	1.11E − 05	4.61	4.07E − 05	4.44
160	6.71E − 07	4.50	2.37E − 06	4.16	5.70E − 07	4.28	2.08E − 06	4.29
320	3.64E − 08	4.20	1.31E − 07	4.18	3.30E − 08	4.11	1.18E − 07	4.14
640	2.13E − 09	4.09	7.56E − 09	4.11	2.01E − 09	4.04	7.08E − 09	4.06

We start with an isentropic initial condition, with a shock at $x = 0.5$. The density ρ and pressure p at $-\infty$ are 1, and the inlet Mach number at $x = 0$ is 0.8. The outlet Mach number at $x = 1$ is 1.8, with linear Mach number distribution before and after the shock. The area of the cross-section $a(x)$ is then determined by the relation

$$a(x)f(\text{Mach number at } x) = \text{constant} \quad \forall x \in [0, 1],$$

where

$$f(w) = \frac{w}{(1 + \delta w^2)^p}, \quad \delta = \frac{1}{2}(\gamma - 1), \quad p = \frac{1}{2} \cdot \frac{\gamma + 1}{\gamma - 1}.$$

From Fig. 3, we can see that the shock is resolved well. Also, we can observe in Table 3 that the design fourth order accuracy can be achieved outside three cells around the shock for non-smooth meshes if we approximate the integral in the shocked cell in two parts separated by the shock, that is, if the shock x_s is within $[x_i, x_{i+1}]$, then the integrals over $[x_i, x_s]$ and over $[x_s, x_{i+1}]$ are approximated separately using WENO

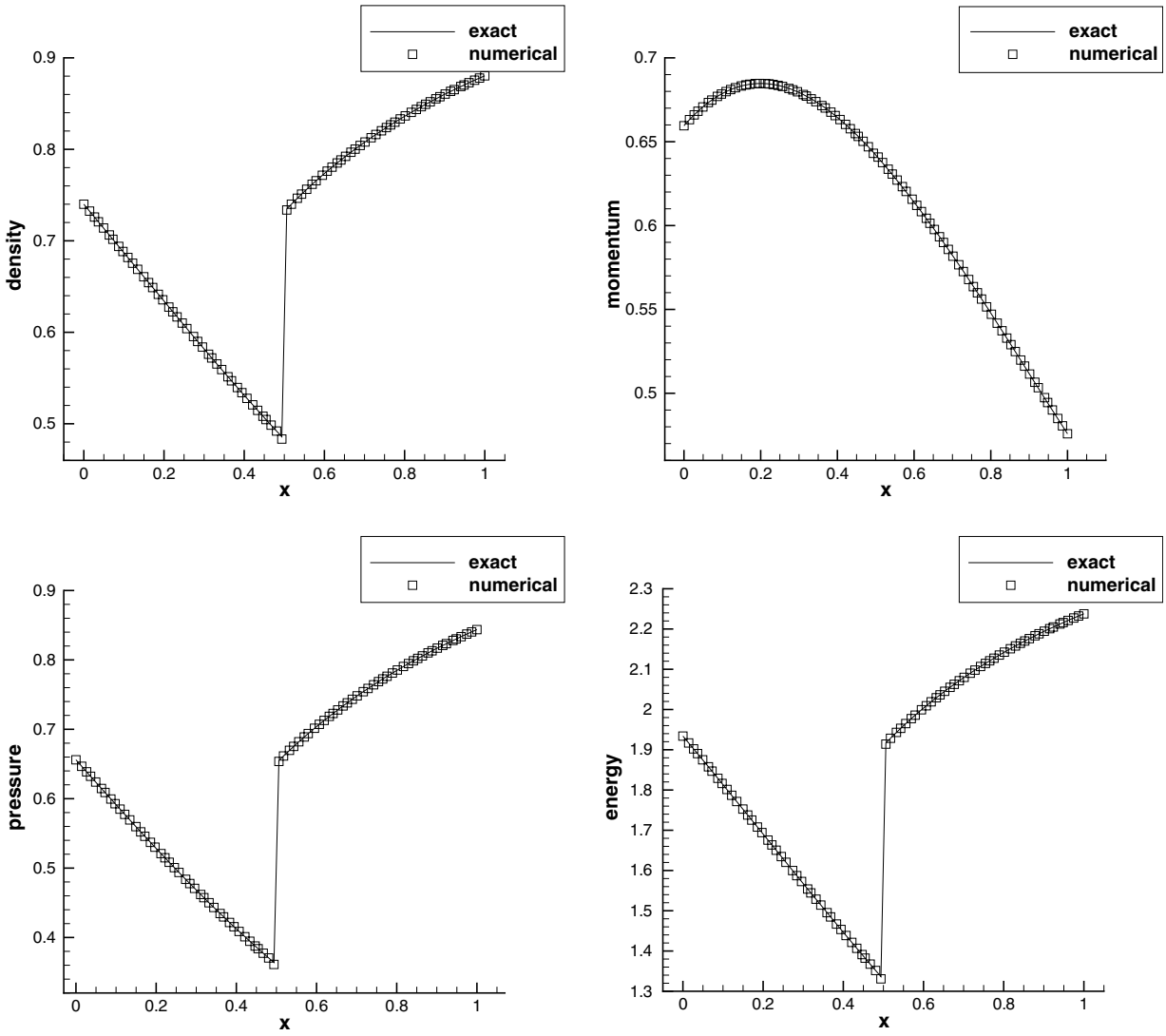

Fig. 3. Nozzle flow problem. Non-smooth mesh with 81 cells. Solid lines: exact solution; symbols: numerical solution. Top left: density; top right: momentum; bottom left: pressure; bottom right: total energy.

Table 3
Errors outside three cells around the shock and numerical orders of accuracy for the density ρ of the fourth order RD finite difference WENO scheme for Example 5.2.2 on non-smooth meshes with N cells

N	Before shock				After shock			
	L^1 error	Order	L^∞ error	Order	L^1 error	Order	L^∞ error	Order
Sub-cell separate integrations in the shocked cell								
21	1.36E − 07	–	7.09E − 07	–	7.58E − 06	–	3.35E − 05	–
41	1.44E − 08	3.23	6.13E − 08	3.53	5.08E − 07	3.90	2.19E − 06	3.93
81	1.28E − 09	3.49	4.85E − 09	3.66	1.67E − 08	4.93	6.61E − 08	5.05
161	8.34E − 11	3.94	3.11E − 10	3.96	7.72E − 10	4.43	3.00E − 09	4.46
321	5.41E − 12	3.95	2.00E − 11	3.96	3.65E − 11	4.40	1.36E − 10	4.46
641	2.22E − 13	4.60	1.20E − 12	4.05	1.75E − 12	4.38	4.92E − 12	4.80
Regular integration in the shocked cell								
21	1.36E − 07	–	7.09E − 07	–	1.75E − 05	–	6.42E − 05	–
41	1.44E − 08	3.24	6.13E − 08	3.53	4.38E − 06	1.99	1.42E − 05	2.18
81	1.28E − 09	3.49	4.85E − 09	3.66	1.11E − 06	1.98	3.37E − 06	2.07
161	8.34E − 11	3.94	3.11E − 10	3.96	2.34E − 07	2.25	7.29E − 07	2.21
321	5.41E − 12	3.95	2.00E − 11	3.96	5.81E − 08	2.01	1.77E − 07	2.04
641	2.22E − 13	4.61	1.22E − 12	4.04	8.15E − 09	2.83	2.52E − 08	2.81

with one-sided stencils (but always including the points x_i and x_{i+1}). This is an idea of sub-cell resolution [16] and requires an accurate estimate of the shock location x_s, which we take as the exact shock location in our numerical experiment. If we perform the approximation of the integral in the shocked cell in the usual way, we would lose some accuracy in the downstream due to error pollution, as shown in the lower half of the table. We refer to [14] for more discussions on such accuracy issues for high order WENO methods applied to systems with shocks. Notice that we have put the exact shock location at the center of a cell for all the meshes.

5.3. Two-dimensional scalar problems

In this section, numerical steady state is obtained with L^1 residue reduced to the round-off level.

Example 5.3.1. We solve the steady state problem of two-dimensional Burgers equation with a source term

$$u_t + \left(\frac{1}{\sqrt{2}}\frac{u^2}{2}\right)_x + \left(\frac{1}{\sqrt{2}}\frac{u^2}{2}\right)_y = \sin\left(\frac{x+y}{\sqrt{2}}\right)\cos\left(\frac{x+y}{\sqrt{2}}\right), \quad (x,y) \in \left[0,\frac{\pi}{\sqrt{2}}\right] \times \left[0,\frac{\pi}{\sqrt{2}}\right] \tag{5.6}$$

with the initial condition given by

$$u(x,y,0) = \beta \sin\left(\frac{x+y}{\sqrt{2}}\right). \tag{5.7}$$

This is the one-dimensional problem in Example 5.1.1 along the northeast–southwest diagonal line. Here, we use the exact solution of the steady state problem as boundary conditions. We have also experimented with the exact solution on the inflow boundaries and extrapolation of the point values with fourth order accuracy on the outflow boundaries, obtaining similar results.

Since our grids are not aligned with the diagonal line, this is a truly two-dimensional test case. For this example we take $\beta = 1.2$, which gives a smooth steady state solution $u(x,y,\infty) = \sin\left(\frac{x+y}{\sqrt{2}}\right)$. For this example, the parameter ε in (3.4) for Roe's entropy correction is taken as 0. We test our scheme on both uniform meshes and non-smooth meshes which are 20% randomly perturbed from the uniform ones. For an example of the non-smooth randomly perturbed mesh, see Fig. 4. The numerical results are shown in Table 4. We can see clearly that fourth order accuracy is achieved and the magnitudes of the errors on these two types of meshes are comparable.

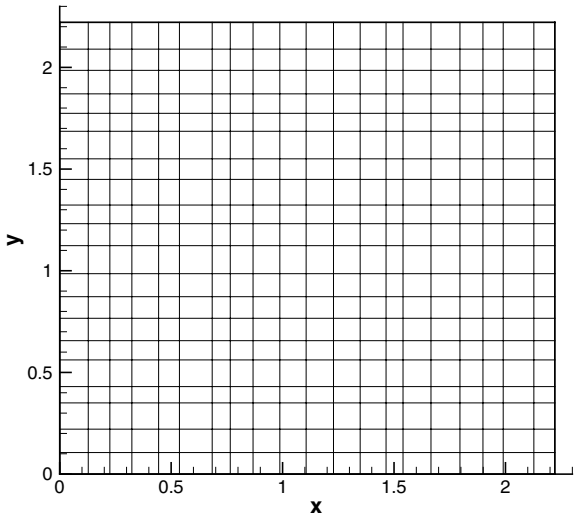

Fig. 4. A demonstration of the non-smooth mesh with 20×20 cells.

Table 4
Errors and numerical orders of accuracy of the fourth order RD finite difference WENO scheme for Example 5.3.1 on non-smooth and uniform meshes with $N \times N$ cells

$N \times N$	Non-smooth mesh				Uniform mesh			
	L^1 error	Order	L^∞ error	Order	L^1 error	Order	L^∞ error	Order
20×20	1.62E − 06	–	5.25E − 06	–	1.63E − 06	–	5.15E − 06	–
40×40	1.22E − 07	3.73	3.28E − 07	4.00	1.15E − 07	3.82	2.98E − 07	4.11
80×80	8.31E − 09	3.88	1.96E − 08	4.06	7.83E − 09	3.88	1.83E − 08	4.03
160×160	5.49E − 10	3.92	1.22E − 09	4.00	5.13E − 10	3.93	1.14E − 09	4.01
320×320	3.52E − 11	3.96	7.63E − 11	4.00	3.23E − 11	3.99	7.09E − 11	4.00

Example 5.3.2. We consider the steady state solution of the following problem:

$$u_t + \left(\frac{1}{\sqrt{2}}\frac{u^2}{2}\right)_x + \left(\frac{1}{\sqrt{2}}\frac{u^2}{2}\right)_y = -\pi \cos\left(\pi \frac{x+y}{\sqrt{2}}\right) u, \quad (x,y) \in \left[0, \frac{1}{\sqrt{2}}\right] \times \left[0, \frac{1}{\sqrt{2}}\right]. \tag{5.8}$$

This is the one-dimensional problem in Example 5.1.3 along the northeast–southwest diagonal line. Inflow boundary conditions are given by the exact solution of the steady state problem. Again, since our grids are not aligned with the diagonal line, this is a truly two-dimensional test case. As before, this problem has two steady state solutions with shocks

$$u(x,y,\infty) = \begin{cases} 1 - \sin\left(\pi \frac{x+y}{\sqrt{2}}\right) & \text{if } 0 \leqslant \frac{x+y}{\sqrt{2}} < x_s, \\ -0.1 - \sin\left(\pi \frac{x+y}{\sqrt{2}}\right) & \text{if } x_s \leqslant \frac{x+y}{\sqrt{2}} < 1, \end{cases}$$

where $x_s = 0.1486$ or $x_s = 0.8514$. Both solutions satisfy the Rankine–Hugoniot jump condition and the entropy conditions, but only the one with the shock at $\frac{x+y}{\sqrt{2}} = 0.1486$ is stable for small perturbation.

The initial condition is given by

$$u(x,y,0) = \begin{cases} 1 & \text{if } 0 \leqslant \frac{x+y}{\sqrt{2}} < 0.5, \\ -0.1 & \text{if } 0.5 \leqslant \frac{x+y}{\sqrt{2}} < 1, \end{cases}$$

where the initial jump is located in the middle of the positions of the shocks in the two admissible steady state solutions. We test our scheme on a non-smooth mesh which is 20% perturbed from the uniform one. The

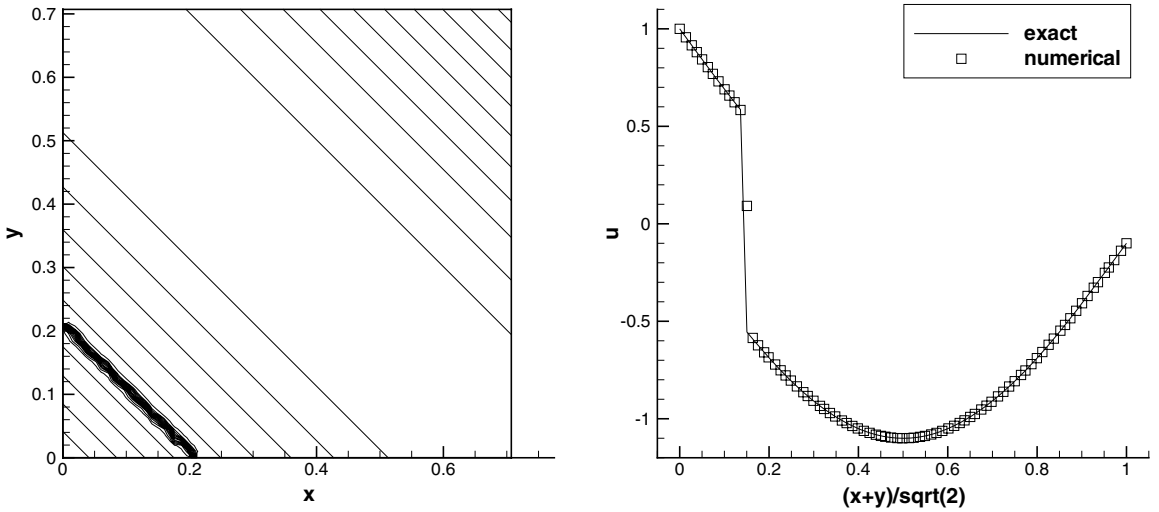

Fig. 5. Example 5.3.2. Non-smooth mesh with 80×80 cells. Left: 25 equally spaced contours of the solution from -1.2 to 1.1; right: the numerical solution (symbols) versus the exact solution (solid line) along the cross-section through the northeast to southwest diagonal.

coefficient δ for the dissipation (4.4) is taken as 10. The numerical result is displayed in Fig. 5. We can see the correct shock location and a good resolution of the solution.

Example 5.3.3. We consider the one-dimensional Burgers equation viewed as a two-dimensional steady state problem

$$u_t + \left(\frac{u^2}{2}\right)_x + u_y = 0, \quad (x,y) \in [0,1] \times [0,1] \tag{5.9}$$

with the boundary conditions

$$u(x,0,t) = 1.5 - 2x, \quad u(0,y,t) = 1.5, \quad u(1,y,t) = -0.5.$$

This problem was studied in [9] as a prototype example for shock boundary layer interaction. We start from an initial condition $u(x,y,0) = u(x,0,0)$ and march to steady state by a pseudo-time marching. The isolines of the numerical solution and the cross-sections for $y = 0.25$ across the fan, for $y = 0.5$ right at the junction where the fan becomes a single shock, and at $y = 0.75$ across the shock, are displayed in Fig. 6. We can clearly observe good resolution of the numerical scheme for this example. The coefficient δ for the dissipation (4.4) is taken as 10.

5.4. Two-dimensional systems

Example 5.4.1. We consider a Cauchy–Riemann problem

$$\frac{\partial W}{\partial t} + A\frac{\partial W}{\partial x} + B\frac{\partial W}{\partial y} = 0, \quad (x,y) \in [-2,2] \times [-2,2], \quad t > 0, \tag{5.10}$$

where

$$A = \begin{pmatrix} 1 & 0 \\ 0 & -1 \end{pmatrix} \quad \text{and} \quad B = \begin{pmatrix} 0 & 1 \\ 1 & 0 \end{pmatrix}$$

with the following Riemann data $W = (u,v)^{\mathrm{T}}$:

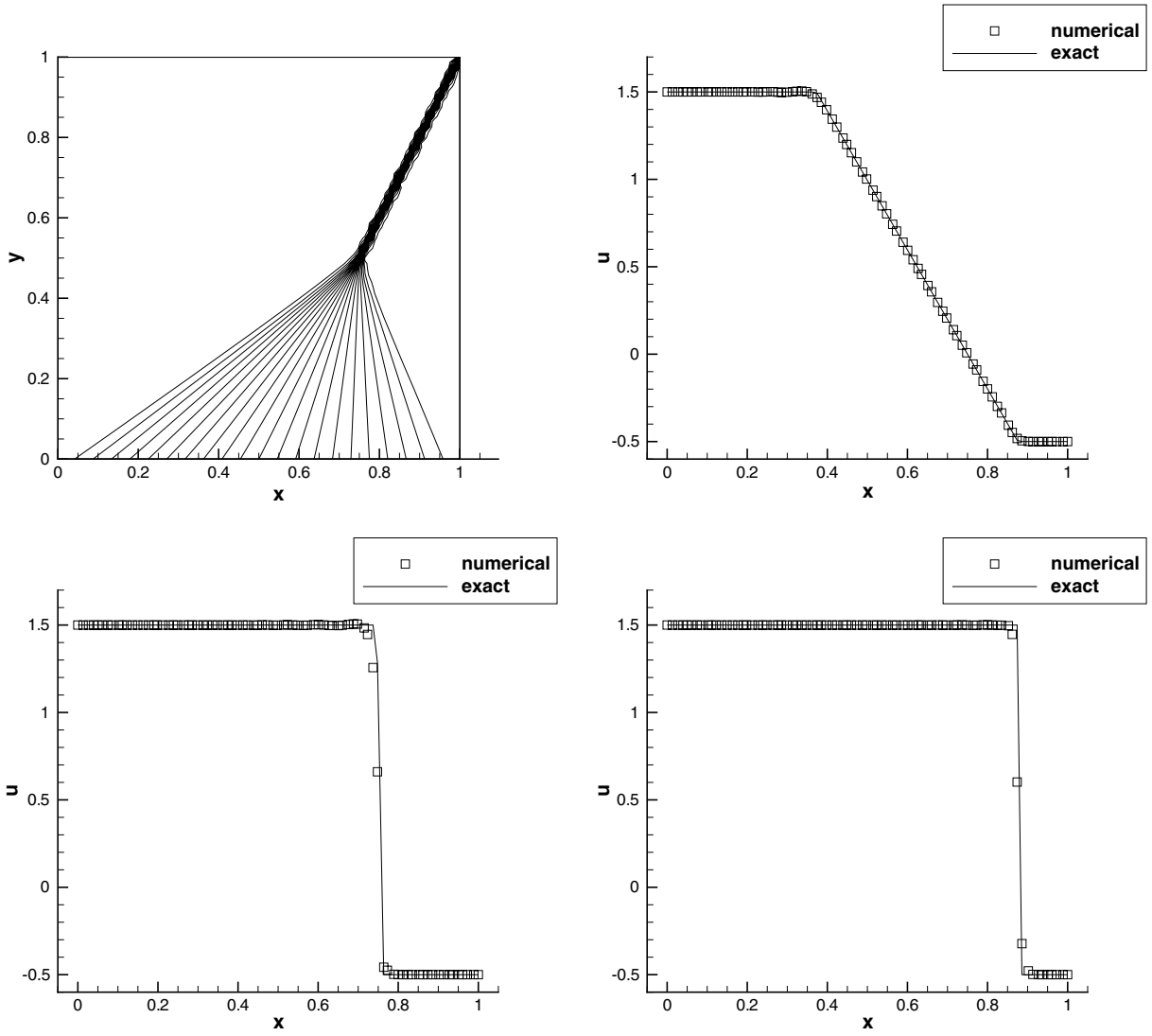

Fig. 6. Example 5.3.3. Non-smooth mesh with 80×80 cells. Top left: 25 equally spaced contour lines from -0.6 to 1.6. Top right: cross-section at $y = 0.25$; bottom left: cross-section at $y = 0.5$; bottom right: cross-section at $y = 0.75$. For the cross-sections, the solid lines are for the exact solution and symbols are for the numerical solution.

$$u = \begin{cases} 1 & \text{if } x > 0 \text{ and } y > 0, \\ -1 & \text{if } x < 0 \text{ and } y > 0, \\ -1 & \text{if } x > 0 \text{ and } y < 0, \\ 1 & \text{if } x < 0 \text{ and } y < 0 \end{cases} \quad \text{and} \quad v = \begin{cases} 1 & \text{if } x > 0 \text{ and } y > 0, \\ -1 & \text{if } x < 0 \text{ and } y > 0, \\ -1 & \text{if } x > 0 \text{ and } y < 0, \\ 2 & \text{if } x < 0 \text{ and } y < 0. \end{cases} \tag{5.11}$$

The solution is self-similar, and therefore $W(x, y, t) = \tilde{W}\left(\frac{x}{t}, \frac{y}{t}\right)$. Let $\xi = \frac{x}{t}$, $\eta = \frac{y}{t}$, then $\tilde{W}$ satisfies

$$(-\xi I + A)\frac{\partial \tilde{W}}{\partial \xi} + (-\eta I + B)\frac{\partial \tilde{W}}{\partial \eta} = 0, \tag{5.12}$$

which can be written as

$$\frac{\partial}{\partial \xi}[(-\xi I + A)\tilde{W}] + \frac{\partial}{\partial \eta}[(-\eta I + B)\tilde{W}] = -2\tilde{W} \tag{5.13}$$

with the boundary conditions at infinity given by the Riemann data in (5.10) and (5.11) at time $t = 1$. Eq. (5.13) can be solved by the pseudo-time marching scheme with the prescribed boundary condition and the same initial condition as in (5.11). The numerical results are shown in Fig. 7. The resolution of the numerical scheme for this problem is very good. The coefficient δ for the dissipation (4.4) is taken as 1. In this case, the L^1 residue can only be reduced to the level around 10^{-6} and then stagnates at that level.

Example 5.4.2. We consider a regular shock reflection problem of the steady state solution of the two-dimensional Euler equations

$$\mathbf{u}_t + \mathbf{f}(\mathbf{u})_x + \mathbf{g}(\mathbf{u})_y = 0, \quad (x, y) \in [0, 4] \times [0, 1], \tag{5.14}$$

where $\mathbf{u} = (\rho, \rho u, \rho v, E)^{\mathrm{T}}$, $\mathbf{f}(\mathbf{u}) = (\rho u, \rho u^2 + p, \rho uv, u(E + p))^{\mathrm{T}}$, and $\mathbf{g}(\mathbf{u}) = (\rho v, \rho uv, \rho v^2 + p, v(E + p))^{\mathrm{T}}$. Here ρ is the density, (u, v) is the velocity, E is the total energy and $p = (\gamma - 1)\left(E - \frac{1}{2}(\rho u^2 + \rho v^2)\right)$ is the pressure. γ is the gas constant which is again taken as 1.4 in our numerical tests.

We start with an initial condition where $(\rho, u, v, p) = (1.69997, 2.61934, -0.50632, 1.52819)$ on $y = 4$ and $(\rho, u, v, p) = (1, 2.9, 0, \frac{1}{\gamma})$ otherwise. The boundary conditions are given by $(\rho, u, v, p) = (1.69997, 2.61934, -0.50632, 1.52819)$ on $y = 4$, and reflective boundary condition on $y = 0$. The left boundary at $x = 0$ is set as an inflow with $(\rho, u, v, p) = (1, 2.9, 0, \frac{1}{\gamma})$, and the right boundary at $x = 4$ is set to be an outflow with no boundary conditions prescribed (one-sided WENO integration is performed near the right boundary). The coefficient δ for the dissipation (4.4) is taken as 10. Numerical steady state is obtained with L^1 residue reduced to the round-off level for this problem. For the convergence history of the L^1 residue, see Fig. 8 (the dash-dot line).

The numerical results are shown in Fig. 9. We can clearly see a good resolution of the incident and reflected shocks.

Example 5.4.3. We consider the same shock reflection problem as in the previous example, but use a different mesh. Our choice for the new mesh is non-Cartesian and consists of parallelograms, and is almost aligned with the shocks, as shown in the left graph of Fig. 10. We can see in the right graph of Fig. 10 that the shocks are well resolved by a coarse 60×30 mesh. This demonstrates the capability of algorithm for non-Cartesian meshes. In this case, the L^1 residue can only be reduced to the level around 10^{-4} and then stagnates at that level. For the convergence history of the L^1 residue, see Fig. 8 (the solid line).

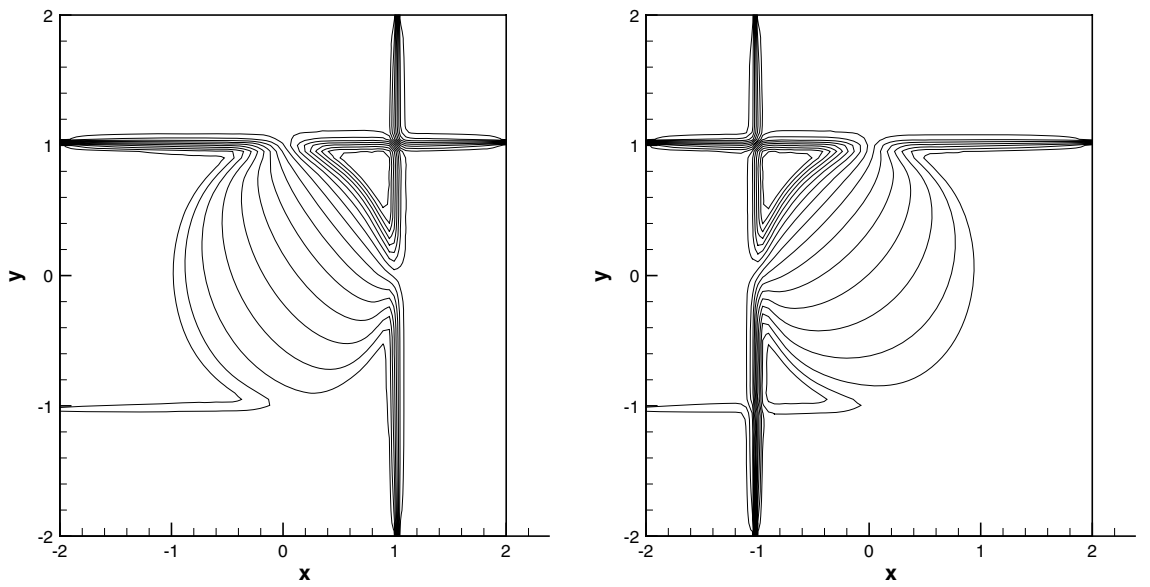

Fig. 7. Example 5.4.1. Non-smooth mesh with 80×80 cells. 20 Equally spaced contours for u from -3 to 1.6 (left) and 20 equally spaced contours for v from -1.6 to 3.5 (right).

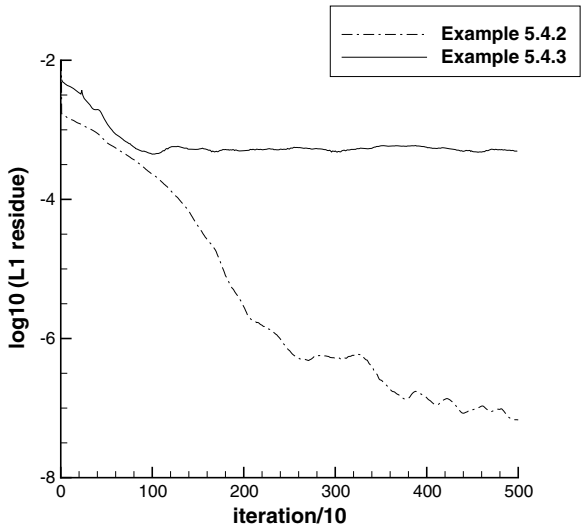

Fig. 8. The L^1 residues of Example 5.4.2 (dash-dot line) and Example 5.4.3 (solid line).

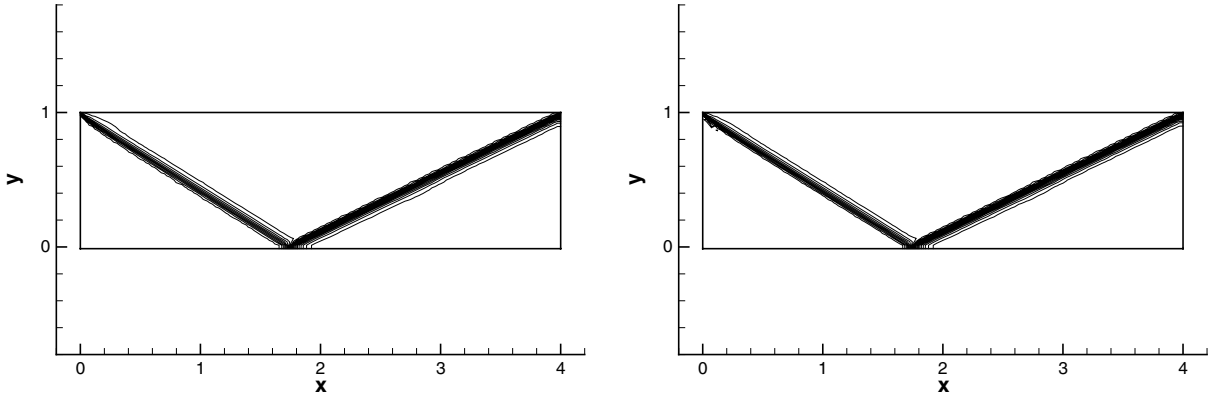

Fig. 9. Shock reflection. 160×40 Non-smooth mesh. Left: 23 equally spaced contours from 0.94 to 2.72 for the density; right: 25 equally spaced contours from 5 to 15.2 for the energy.

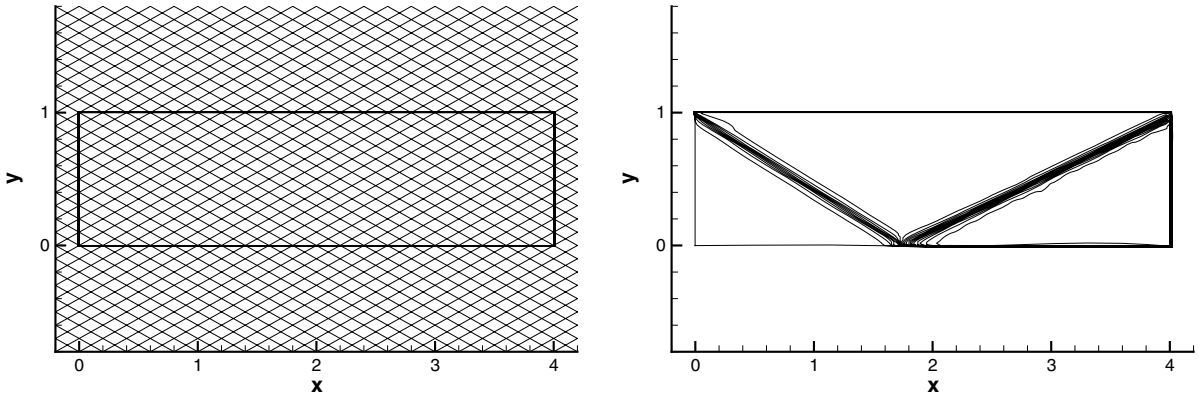

Fig. 10. Shock reflection. Non-Cartesian mesh with 60×30 cells. Left: a demonstration of the mesh with 20×10 cells; right: 23 equally spaced contours from 0.94 to 2.72 for the density.

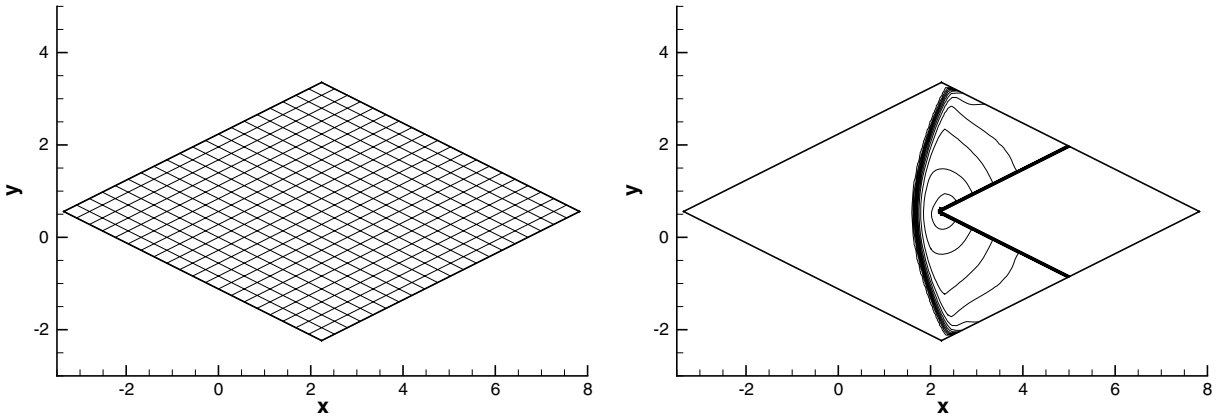

Fig. 11. Example 5.4.4. Flow passing a wedge. Non-Cartesian mesh with 80×80 cells. Left: a demonstration of the mesh with 20×20 cells; right: 20 equally spaced contours from 0 to 2.6 for the density.

Example 5.4.4. We solve the problem of flow passing a wedge with a 60° angle. Steady state solution of the Euler equations (5.14) is computed with the initial condition taken as $\rho = 1$, $p = 1/1.4$, $(u, v) = (1.8, 0)$ which is a Mach 1.8 flow. The boundary conditions are set to be reflective on both sides of the wedge. We use a non-Cartesian mesh consisting of parallelograms, which is aligned with the two sides of the wedge, as shown in the left graph of Fig. 11. This is an easier setup than the multi-domain finite difference setup in [19], albeit with difficulties in the implementation of reflective boundary conditions along the wedge except for special angles such as the 60° angle that we have tested. In the right hand side of Fig. 11, we can see that the shock is resolved well. In this case, the L^1 residue can only be reduced to the level around 10^{-4} and then stagnates at that level.

6. Concluding remarks

In this paper, we have designed a high order residual distribution finite difference WENO scheme on non-smooth Cartesian or general curvilinear meshes for solving steady state solutions of conservation laws in one and two space dimensions. The restriction on the meshes allows us to compute the residual dimension by dimension to high order accuracy, therefore the cost of the algorithm is comparable with that of the high order finite difference WENO schemes and much lower than that of the high order finite volume WENO schemes, yet the new method does not have the requirement for the smoothness of the meshes of the traditional high order conservative finite difference schemes. The idea of residual distribution is adapted and allows us to obtain high order accuracy at steady state. A Lax–Wendroff type theorem is proved for convergence towards weak solutions in one and two dimensions. Numerical examples are given to demonstrate the accuracy and non-oscillatory shock resolution of the proposed scheme. Generalization of the technique to 3D is straightforward and will be carried out in the future. Acceleration techniques to reach steady state more efficiently, improvement on the additional dissipation residual for stabilizing the pseudo time marching, and extension of the method for time accurate problems also constitute future work.

Acknowledgments

Research supported by ARO Grant W911NF-04-1-0291, NSF Grants DMS-0207451 and DMS-0510345, and AFOSR Grant FA9550-05-1-0123.

Appendix A. A Lax–Wendroff type theorem for two dimensions

In this appendix, we state and prove a Lax–Wendroff type theorem for convergence towards weak solutions in two-dimensional scalar case.

We follow the notations in Section 4.1. In addition, we define $S^x_{i+\frac{1}{2}} = \{x | x \in [x_i, x_{i+1}]\}$, $S^y_{j+\frac{1}{2}} = \{y | y \in [y_j, y_{j+1}]\}$, $\Delta x_{i+\frac{1}{2}} = x_{i+1} - x_i$, $\Delta y_{j+\frac{1}{2}} = y_{j+1} - y_j$ and $\Delta x = \max_i \Delta x_i$, $\Delta y = \max_j \Delta y_j$, $\Delta = \max(\Delta x, \Delta y)$. Here, we assume $0 < C_1 \leqslant |\Delta x_{i+\frac{1}{2}} / \Delta y_{j+\frac{1}{2}}| \leqslant C_2$ for all i,j. Also, we define the function $u_{\Delta x,\Delta y}$ as a piecewise constant function where $u_{\Delta x,\Delta y}(x,y) = u_{ij}$, $(x,y) \in C_{ij}$.

As in Section 4.2, the residual in the cell $I_{i+\frac{1}{2},j+\frac{1}{2}}$ given by (4.2) is approximated by

$$\begin{aligned}\Phi_{i+\frac{1}{2},j+\frac{1}{2}} = {} & \mathscr{R}\left(f(u_{\Delta x,\Delta y}(x_{i+1},y)), S^y_{j+\frac{1}{2}}\right) - \mathscr{R}\left(f(u_{\Delta x,\Delta y}(x_i,y)), S^y_{j+\frac{1}{2}}\right) + \mathscr{R}\left(g(u_{\Delta x,\Delta y}(x,y_{j+1})), S^x_{i+\frac{1}{2}}\right) \\ & - \mathscr{R}\left(g(u_{\Delta x,\Delta y}(x,y_j)), S^x_{i+\frac{1}{2}}\right) + \mathscr{R}\left(\mathscr{R}\left(h(u_{\Delta x,\Delta y},x,y), S^y_{j+\frac{1}{2}}\right), S^x_{i+\frac{1}{2}}\right),\end{aligned}$$

where $\mathscr{R}$ is the one-dimensional numerical integration operator, with the first argument as the integrand and the second the integration interval. The integral approximation can be written as a linear combination of the point values of the integrand, as described in Section 2, and therefore the residual with $2r-1$ order accuracy can be represented by

$$\begin{aligned}\Phi_{i+\frac{1}{2},j+\frac{1}{2}} = {} & \sum_{k=-r+2}^{r-1} (a^k_{i+1,j} f(u_{i+1,j+k}) - a^k_{ij} f(u_{i,j+k})) \Delta y_{j+\frac{1}{2}} + \sum_{k=-r+2}^{r-1} (b^k_{i,j+1} g(u_{i+k,j+1}) - b^k_{ij} g(u_{i+k,j})) \Delta x_{i+\frac{1}{2}} \\ & + \mathscr{R}\left(\mathscr{R}\left(h(u_{\Delta x,\Delta y},x,y), S^y_{j+\frac{1}{2}}\right), S^x_{i+\frac{1}{2}}\right),\end{aligned} \tag{A.15}$$

where the coefficients $a^k_{ij} = a^k_{ij}(u_{i,j-r+2}, \ldots, u_{i,j+r-1})$ are Lipschitz continuous functions in all the arguments, and so are b^k_{ij}. For example, the WENO weights used in this paper are Lipschitz continuous since the smoothness indicators are smooth functions of u.

The distributed residuals, as defined in Section 4.1, are $\tilde{\Phi}^k_{i+\frac{1}{2},j+\frac{1}{2}}$, $k = 1, \ldots, 4$, which are revised from the original one by adding a dissipation residual $\theta \Phi^k_{\text{diss}}$ defined in Eq. (4.4), where θ is the local discontinuity indicator. Suppose the residuals satisfy the conservation property, by the fact that $\sum_{k=1}^4 \Phi^k_{\text{diss}} = 0$

$$\Phi_{i+\frac{1}{2},j+\frac{1}{2}} = \sum_{k=1}^4 \tilde{\Phi}^k_{i+\frac{1}{2},j+\frac{1}{2}} = \sum_{k=1}^4 \Phi^k_{i+\frac{1}{2},j+\frac{1}{2}} \tag{A.16}$$

and residual property for the unrevised distributed residuals

$$\frac{\left|\Phi^k_{i+\frac{1}{2},j+\frac{1}{2}}\right|}{\left|\Phi_{i+\frac{1}{2},j+\frac{1}{2}}\right|} \leqslant C, \quad k = 1, \ldots, 4. \tag{A.17}$$

Equipped with properties mentioned above, we have the following theorem.

Theorem A.1. *Assume that the flux function f and g in Eq. (4.1) are Lipschitz continuous, and the source term $h(u,x,y)$ is continuous in all arguments. If $u_{\Delta x,\Delta y}$ is a steady state solution of Eq. (4.6) satisfying Eqs. (A.15)–(A.17) , and there is a function u with bounded total variation such that*

$$u_{\Delta x,\Delta y} \to u \quad \text{in } L^1(\mathbb{R}^2) \quad \text{as } \Delta x, \Delta y \to 0$$

and

$$\sup_{\Delta x,\Delta y} \sup_{x,y} |u_{\Delta x,\Delta y}(x,y)| \leqslant C,$$

then u is a weak solution to Eq. (4.1).

Proof. At steady state of the scheme, $\tilde{\Phi}^1_{i-\frac{1}{2},j-\frac{1}{2}} + \tilde{\Phi}^2_{i-\frac{1}{2},j+\frac{1}{2}} + \tilde{\Phi}^3_{i+\frac{1}{2},j-\frac{1}{2}} + \tilde{\Phi}^4_{i+\frac{1}{2},j+\frac{1}{2}} = 0$ for all i,j. Let $\varphi \in C^\infty_0(\mathbb{R}^2)$ be a test function, denote $\varphi_{ij} = \varphi(x_i, y_j)$, and define $\theta_{i+\frac{1}{2},j} = \frac{\theta_{i+\frac{1}{2},j+\frac{1}{2}} + \theta_{i+\frac{1}{2},j-\frac{1}{2}}}{2}$ and $\theta_{i,j+\frac{1}{2}} = \frac{\theta_{i-\frac{1}{2},j+\frac{1}{2}} + \theta_{i+\frac{1}{2},j+\frac{1}{2}}}{2}$. We have

$$
\begin{aligned}
0 &= \sum_{i,j}\left(\tilde{\Phi}^1_{i-\frac{1}{2},j-\frac{1}{2}}+\tilde{\Phi}^2_{i-\frac{1}{2},j+\frac{1}{2}}+\tilde{\Phi}^3_{i+\frac{1}{2},j-\frac{1}{2}}+\tilde{\Phi}^4_{i+\frac{1}{2},j+\frac{1}{2}}\right)\varphi_{ij}\\
&= \sum_{i,j}\left(\Phi^1_{i-\frac{1}{2},j-\frac{1}{2}}+\Phi^2_{i-\frac{1}{2},j+\frac{1}{2}}+\Phi^3_{i+\frac{1}{2},j-\frac{1}{2}}+\Phi^4_{i+\frac{1}{2},j+\frac{1}{2}}\right)\varphi_{ij}+\delta\Delta^3\\
&\quad\times\sum_{i,j}\left(\theta_{i-\frac{1}{2},j}\frac{u_{ij}-u_{i-1,j}}{\Delta x_{i-\frac{1}{2}}}+\theta_{i+\frac{1}{2},j}\frac{u_{ij}-u_{i+1,j}}{\Delta x_{i+\frac{1}{2}}}+\theta_{i,j-\frac{1}{2}}\frac{u_{ij}-u_{i,j-1}}{\Delta y_{j-\frac{1}{2}}}+\theta_{i,j+\frac{1}{2}}\frac{u_{ij}-u_{i,j+1}}{\Delta y_{j+\frac{1}{2}}}\right)\varphi_{ij}\\
&= \sum_{i,j}\Phi_{i-\frac{1}{2},j-\frac{1}{2}}\varphi_{ij}-\sum_{i,j}\Phi^2_{i-\frac{1}{2},j+\frac{1}{2}}(\varphi_{i,j+1}-\varphi_{ij})-\sum_{i,j}\Phi^3_{i+\frac{1}{2},j-\frac{1}{2}}(\varphi_{i+1,j}-\varphi_{ij})-\sum_{i,j}\Phi^4_{i+\frac{1}{2},j+\frac{1}{2}}(\varphi_{i+1,j+1}-\varphi_{ij})+\delta\Delta^3\\
&\quad\times\sum_{i,j}\left(\theta_{i-\frac{1}{2},j}\frac{u_{ij}-u_{i-1,j}}{\Delta x_{i-\frac{1}{2}}}+\theta_{i+\frac{1}{2},j}\frac{u_{ij}-u_{i+1,j}}{\Delta x_{i+\frac{1}{2}}}+\theta_{i,j-\frac{1}{2}}\frac{u_{ij}-u_{i,j-1}}{\Delta y_{j-\frac{1}{2}}}+\theta_{i,j+\frac{1}{2}}\frac{u_{ij}-u_{i,j+1}}{\Delta y_{j+\frac{1}{2}}}\right)\varphi_{ij}\\
&= \mathrm{I}+\mathrm{II}+\mathrm{III}+\mathrm{IV}+\mathrm{V}.
\end{aligned}
$$

We look at the first summation term,

$$
\begin{aligned}
\mathrm{I} &= \sum_{i,j}\Phi_{i-\frac{1}{2},j-\frac{1}{2}}\varphi_{ij}\\
&= \sum_{i,j}\sum_{k=-r+2}^{r-1}\left(a^k_{ij}f(u_{i,j+k})-a^k_{i-1,j}f(u_{i-1,j+k})\right)\Delta y_{j+\frac{1}{2}}\varphi_{i,j+1}\\
&\quad+\sum_{i,j}\sum_{k=-r+2}^{r-1}\left(b^k_{ij}g(u_{i+k,j})-b^k_{i,j-1}g(u_{i+k,j-1})\right)\Delta x_{i+\frac{1}{2}}\varphi_{i+1,j}-\sum_{i,j}\mathscr{R}\left(\mathscr{R}\left(h(u_{\Delta x,\Delta y},x,y),S^y_{j-\frac{1}{2}}\right),S^x_{i-\frac{1}{2}}\right)\varphi_{ij}\\
&= -\sum_{i,j}\sum_{k=-r+2}^{r-1}a^k_{ij}f(u_{i,j+k})\frac{\varphi_{i+1,j+1}-\varphi_{i,j+1}}{\Delta x_{i+\frac{1}{2}}}\Delta x_{i+\frac{1}{2}}\Delta y_{j+\frac{1}{2}}-\sum_{i,j}\sum_{k=-r+2}^{r-1}b^k_{ij}g(u_{i+k,j})\frac{\varphi_{i+1,j+1}-\varphi_{i+1,j}}{\Delta y_{j+\frac{1}{2}}}\Delta y_{j+\frac{1}{2}}\Delta x_{i+\frac{1}{2}}\\
&\quad-\sum_{i,j}\mathscr{R}\left(\mathscr{R}\left(h(u_{\Delta x,\Delta y},x,y),S^y_{j-\frac{1}{2}}\right),S^x_{i-\frac{1}{2}}\right)\varphi_{ij}\\
&= -\sum_{i}\sum_{j}\mathscr{R}\left(f(u_{\Delta x,\Delta y},x_i,y),S^y_{j+\frac{1}{2}}\right)\frac{\varphi_{i+1,j+1}-\varphi_{i,j+1}}{\Delta x_{i+\frac{1}{2}}}\Delta x_{i+\frac{1}{2}}\\
&\quad-\sum_{j}\sum_{i}\mathscr{R}\left(g(u_{\Delta x,\Delta y},x,y_j),S^x_{i+\frac{1}{2}}\right)\frac{\varphi_{i+1,j+1}-\varphi_{i+1,j}}{\Delta y_{j+\frac{1}{2}}}\Delta y_{j+\frac{1}{2}}-\sum_{i,j}\mathscr{R}\left(\mathscr{R}\left(h(u_{\Delta x,\Delta y},x,y),S^y_{j-\frac{1}{2}}\right),S^x_{i-\frac{1}{2}}\right)\varphi_{ij}.
\end{aligned}
$$

Note that:

$$
\begin{aligned}
&-\sum_{i}\sum_{j}\mathscr{R}\left(f(u_{\Delta x,\Delta y},x_i,y),S^y_{j+\frac{1}{2}}\right)\frac{\varphi_{i+1,j+1}-\varphi_{i,j+1}}{\Delta x_{i+\frac{1}{2}}}\Delta x_{i+\frac{1}{2}}\to-\int\int f(u)\varphi_x\,\mathrm{d}x\,\mathrm{d}y\quad\text{as }\Delta x,\Delta y\to 0,\\
&-\sum_{j}\sum_{i}\mathscr{R}\left(g(u_{\Delta x,\Delta y},x,y_j),S^x_{i+\frac{1}{2}}\right)\frac{\varphi_{i+1,j+1}-\varphi_{i+1,j}}{\Delta y_{j+\frac{1}{2}}}\Delta y_{j+\frac{1}{2}}\to-\int\int g(u)\varphi_y\,\mathrm{d}x\,\mathrm{d}y\quad\text{as }\Delta x,\Delta y\to 0,\\
&-\sum_{i,j}\mathscr{R}\left(\mathscr{R}\left(h(u_{\Delta x,\Delta y},x,y),S^y_{j-\frac{1}{2}}\right),S^x_{i-\frac{1}{2}}\right)\varphi_{ij}\to\int\int h(u,x,y)\varphi\,\mathrm{d}x\,\mathrm{d}y\quad\text{as }\Delta x,\Delta y\to 0.
\end{aligned}
$$

Therefore,

$$
\mathrm{I}\to-\int\int f(u)\varphi_x\,\mathrm{d}x\,\mathrm{d}y-\int\int g(u)\varphi_y\,\mathrm{d}x\,\mathrm{d}y-\int\int h(u,x,y)\varphi\,\mathrm{d}x\,\mathrm{d}y\quad\text{as }\Delta x,\Delta y\to 0.
$$

Next, we estimate the second term II:

$$
\begin{aligned}
|\mathrm{II}| &= \left|\sum_{i,j} \Phi^2_{i-\frac{1}{2},j+\frac{1}{2}}(\varphi_{i,j+1}-\varphi_{ij})\right| \leqslant \sum_{i,j}\left|\Phi^2_{i-\frac{1}{2},j+\frac{1}{2}}\right||\varphi_{i,j+1}-\varphi_{ij}| \leqslant C\sum_{i,j}\left|\Phi_{i-\frac{1}{2},j+\frac{1}{2}}\right||\varphi_{i,j+1}-\varphi_{ij}| \\
&\leqslant C\sum_{i,j}\sum_{k=-r+2}^{r-1}|a^k_{ij}f(u_{i,j+k})-a^k_{i-1,j}f(u_{i-1,j+k})||\varphi_{i,j+1}-\varphi_{ij}|\Delta y \\
&\quad + C\sum_{i,j}\sum_{k=-r+2}^{r-1}|b^k_{i,j+1}g(u_{i+k,j+1})-b^k_{ij}g(u_{i+k,j})||\varphi_{i,j+1}-\varphi_{ij}|\Delta x \\
&\quad + \sum_{i,j}\mathscr{R}\left(\mathscr{R}\left(|h(u_{\Delta x,\Delta y},x,y)|,S^y_{j+\frac{1}{2}}\right),S^x_{i-\frac{1}{2}}\right)|\varphi_{i,j+1}-\varphi_{i,j}| \\
&\leqslant C\sum_{i,j}\sum_{k=-r+2}^{r-1}|a^k_{ij}||f(u_{i,j+k})-f(u_{i-1,j+k})||\varphi_{i,j+1}-\varphi_{ij}|\Delta y \\
&\quad + C\sum_{i,j}\sum_{k=-r+2}^{r-1}|a^k_{ij}-a^k_{i-1,j}||f(u_{i-1,j+k})||\varphi_{i,j+1}-\varphi_{ij}|\Delta y \\
&\quad + C\sum_{i,j}\sum_{k=-r+2}^{r-1}|b^k_{i,j+1}||g(u_{i+k,j+1})-g(u_{i+k,j})||\varphi_{i,j+1}-\varphi_{ij}|\Delta x \\
&\quad + C\sum_{i,j}\sum_{k=-r+2}^{r-1}|b^k_{i,j+1}-b^k_{i,j}||g(u_{i+k,j})||\varphi_{i,j+1}-\varphi_{ij}|\Delta x \\
&\quad + \sum_{i,j}\mathscr{R}\left(\mathscr{R}\left(|h(u_{\Delta x,\Delta y},x,y)|,S^y_{j+\frac{1}{2}}\right),S^x_{i-\frac{1}{2}}\right)|\varphi_{i,j+1}-\varphi_{i,j}|.
\end{aligned}
$$

Since $\int\int |h(u,x,y)||\varphi_y|\,\mathrm{d}x\,\mathrm{d}y$ is bounded, $\sum_{i,j}\mathscr{R}\left(\mathscr{R}\left(|h(u_{\Delta x,\Delta y},x,y)|,S^y_{j+\frac{1}{2}}\right),S^x_{i+\frac{1}{2}}\right)\left|\frac{\varphi_{i,j+1}-\varphi_{i,j}}{\Delta y_{j+\frac{1}{2}}}\right|$ is bounded, hence the last term above is of the size $\mathrm{O}(\Delta y)$. Also, due to Lipschitz continuity of a^k_{ij}, b^k_{ij} and the flux functions, and boundedness of u_{ij} and $0 < C_1 \leqslant \left|\Delta x_{i+\frac{1}{2}}/\Delta y_{j+\frac{1}{2}}\right| \leqslant C_2$, we have

$$
|\mathrm{II}| \leqslant C_3\sum_{i,j}|u_{i,j}-u_{i-1,j}|\Delta x\Delta y + C_3\sum_{i,j}|u_{i,j}-u_{i,j-1}|\Delta x\Delta y + \mathrm{O}(\Delta y). \tag{A.18}
$$

The first term on the right side of (A.18) can be estimated by

$$
\begin{aligned}
\sum_{i,j}|u_{i,j}-u_{i-1,j}|\Delta x\Delta y &\leqslant \sum_{i,j}|u_{ij}-u(x_i,y_j)|\Delta x\Delta y + \Delta y\sum_i\sum_j|u(x_i,y_j)-u(x_{i-1},y_j)|\Delta x \\
&\quad + \sum_{i,j}|u(x_{i-1},y_j)-u_{i-1,j}|\Delta x\Delta y
\end{aligned}
$$

and it goes to zero when the mesh is refined due to the L^1 convergence of the numerical solution and the fact that limit solution u has bounded total variation. Similarly, the second term on the right side of (A.18) also goes to zero when the mesh is refined. Therefore, $\mathrm{II} \to 0$ as $\Delta x, \Delta y \to 0$. Similarly, we can easily prove that $\mathrm{III}, \mathrm{IV} \to 0$ as $\Delta x, \Delta y \to 0$.

Lastly,

$$
\begin{aligned}
\mathrm{V} &= \delta\Delta^3\sum_{i,j}\left(\theta_{i-\frac{1}{2},j}\frac{u_{ij}-u_{i-1,j}}{\Delta x_{i-\frac{1}{2}}} - \theta_{i+\frac{1}{2},j}\frac{u_{i+1,j}-u_{i,j}}{\Delta x_{i+\frac{1}{2}}}\right)\varphi_{ij} + \delta\Delta^3\sum_{i,j}\left(\theta_{i,j-\frac{1}{2}}\frac{u_{ij}-u_{i,j-1}}{\Delta y_{j-\frac{1}{2}}} - \theta_{i,j+\frac{1}{2}}\frac{u_{i,j+1}-u_{ij}}{\Delta y_{j+\frac{1}{2}}}\right)\varphi_{ij} \\
&= \delta\Delta^3\sum_{i,j}\theta_{i-\frac{1}{2},j}(u_{ij}-u_{i-1,j})\frac{\varphi_{ij}-\varphi_{i-1,j}}{\Delta x_{i-\frac{1}{2}}} + \delta\Delta^3\sum_{i,j}\theta_{i,j-\frac{1}{2}}(u_{ij}-u_{i,j-1})\frac{\varphi_{ij}-\varphi_{i,j-1}}{\Delta y_{j-\frac{1}{2}}}.
\end{aligned}
$$

Clearly, the boundedness of θ and u_{ij} implies that $|V|$ is bounded by $O(\Delta)$, hence $V \to 0$ as $\Delta \to 0$. We can now conclude that

$$-\int\int f(u)\varphi_x \,dx\,dy - \int\int g(u)\varphi_y \,dx\,dy = \int\int h(u,x,y)\varphi \,dx\,dy$$

so u is a weak solution of Eq. (4.1). □

References

[1] R. Abgrall, Toward the ultimate conservative scheme: following the quest, Journal of Computational Physics 167 (2001) 277–315.
[2] R. Abgrall, Essentially non oscillatory residual distribution schemes for hyperbolic problems, Journal of Computational Physics (submitted for publication).
[3] R. Abgrall, T. Barth, Residual distribution schemes for conservation laws via adaptive quadrature, SIAM Journal of Scientific Computing 24 (2002) 732–769.
[4] R. Abgrall, F. Marpeau, Residual distribution schemes on quadrilateral meshes, Journal of Scientific Computing (in press).
[5] R. Abgrall, K. Mer, B. Nkonga, A Lax–Wendroff type theorem for residual schemes, in: M. Hafez, J.J. Chattot (Eds.), Innovative Methods for Numerical Solutions of Partial Differential Equations, World Scientific, Singapore, 2002, pp. 243–266.
[6] R. Abgrall, M. Mezine, Construction of second order accurate monotone and stable residual distribution schemes for unsteady problems, Journal of Computational Physics 188 (2003) 16–55.
[7] R. Abgrall, M. Mezine, Construction of second order accurate monotone and stable residual distribution schemes for steady problems, Journal of Computational Physics 195 (2004) 474–507.
[8] R. Abgrall, P.L. Roe, High order fluctuation scheme on triangular meshes, Journal of Scientific Computing 19 (2003) 3–36.
[9] W. Cai, D. Gottlieb, C.-W. Shu, Essentially nonoscillatory spectral Fourier methods for shock wave calculations, Mathematics of Computation 52 (1989) 389–410.
[10] J. Casper, C.-W. Shu, H.L. Atkins, Comparison of two formulations for high-order accurate essentially nonoscillatory schemes, AIAA Journal 32 (1994) 1970–1977.
[11] Á. Csík, H. Deconinck, Space-time residual distribution schemes for hyperbolic conservation laws on unstructured linear finite elements, International Journal for Numerical Methods in Fluids 40 (2002) 573–581.
[12] H. Deconinck, R. Struijs, G. Bourgeois, P. Roe, Compact advection schemes on unstructured meshes, Computational Fluid Dynamics (1993), VKI Lecture Series 1993–04.
[13] P. Embid, J. Goodman, A. Majda, Multiple steady states for 1-D transonic flow, SIAM Journal on Scientific and Statistical Computing 5 (1984) 21–41.
[14] S. Gottlieb, D. Gottlieb, C.-W. Shu, Recovering high order accuracy in WENO computations of steady state hyperbolic systems, Journal of Scientific Computing (in press).
[15] A. Harten, High resolution schemes for hyperbolic conservation laws, Journal of Computational Physics 49 (1983) 357–393.
[16] A. Harten, ENO schemes with subcell resolution, Journal of Computational Physics 83 (1989) 148–184.
[17] A. Harten, B. Engquist, S. Osher, S. Chakravathy, Uniformly high order accurate essentially non-oscillatory schemes, III, Journal of Computational Physics 71 (1987) 231–303.
[18] G. Jiang, C.-W. Shu, Efficient implementation of weighted ENO schemes, Journal of Computational Physics 126 (1996) 202–228.
[19] K. Kremeyer, K. Sebastian, C.-W. Shu, Computational study of shock mitigation and drag reduction by pulsed energy lines, AIAA Journal (submitted for publication).
[20] X. Liu, S. Osher, T. Chan, Weighted essentially non-oscillatory schemes, Journal of Computational Physics 115 (1994) 200–212.
[21] B. Merryman, Understanding the Shu–Osher conservative finite difference form, Journal of Scientific Computing 19 (2003) 309–322.
[22] P.L. Roe, Approximate Riemann solvers, parameter vectors, and difference schemes, Journal of Computational Physics 43 (1981) 357–372.
[23] P.L. Roe, D. Sidilkover, Optimum positive linear schemes for advection in two or three dimensions, SIAM Journal of Numerical Analysis 29 (1992) 1542–1588.
[24] M.D. Salas, S. Abarbanel, D. Gottlieb, Multiple steady states for characteristic initial value problems, Applied Numerical Mathematics 2 (1986) 193–210.
[25] K. Sebastian, C.-W. Shu, Multi domain WENO finite difference method with interpolation at sub-domain interfaces, Journal of Scientific Computing 19 (2003) 405–438.
[26] C.-W. Shu, Essentially non-oscillatory and weighted essentially non-oscillatory schemes for hyperbolic conservation laws, in: B. Cockburn, C. Johnson, C.-W. Shu, E. Tadmor (Eds.), Advanced Numerical Approximation of Nonlinear Hyperbolic Equations, in: A. Quarteroni (Ed.), Lecture Notes in Mathematics, vol. 1697, Springer, Germany, 1998, pp. 325–432.
[27] C.-W. Shu, High order finite difference and finite volume WENO schemes and discontinuous Galerkin methods for CFD, International Journal of Computational Fluid Dynamics 17 (2003) 107–118.
[28] C.-W. Shu, S. Osher, Efficient implementation of essentially non-oscillatory shock-capturing schemes, Journal of Computational Physics 77 (1988) 439–471.
[29] C.-W. Shu, S. Osher, Efficient implementation of essentially non-oscillatory shock-capturing schemes, II, Journal of Computational Physics 83 (1989) 32–78.

[30] R. Struijs, H. Deconinck, P.L. Roe, Fluctuation splitting schemes for the 2D Euler equations, Computational Fluid Dynamics (1991), VKI Lecture Series 1991–01.
[31] E. van der Weide, H. Deconinck, Fluctuation splitting schemes for the Euler equations on quadrilateral grids, in: Numerical Methods for Fluid Dynamics V, Oxford, UK, 1995, pp. 623–630.
[32] E. van der Weide, H. Deconinck, Positive matrix distribution schemes for hyperbolic systems, in: Dèsidèri, C. Hirch, P. Le Tallec, M. Pandolfi, J. Pèriaux (Eds.), Computational Fluid Dynamics, Wiley, New York, 1996, pp. 747–753.
[33] Z. Xu, C.-W. Shu, Anti-diffusive flux corrections for high order finite difference WENO schemes, Journal of Computational Physics 205 (2005) 458–485.